Journal Pre-proofs

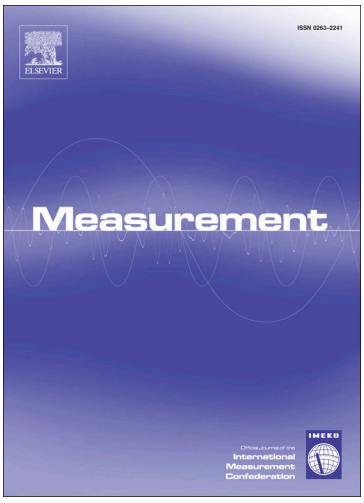

Maximal overlap discrete wavelet packet transforms-based bipolar neutrosophic cross entropy measure for identification of rotor defects

Chander Parkash C.P. Gandhi, Jiawei Xiang, Anil Kumar, Govind Vashishtha, Ravi Kant

PII: S0263-2241(22)00791-6
DOI: https://doi.org/10.1016/j.measurement.2022.111577
Reference: MEASUR 111577

To appear in: *Measurement*

Received Date: 30 April 2022
Revised Date: 19 June 2022
Accepted Date: 27 June 2022

Please cite this article as: C. Parkash C.P. Gandhi, J. Xiang, A. Kumar, G. Vashishtha, R. Kant, Maximal overlap discrete wavelet packet transforms-based bipolar neutrosophic cross entropy measure for identification of rotor defects, *Measurement* (2022), doi: https://doi.org/10.1016/j.measurement.2022.111577

Maximal overlap discrete wavelet packet transforms-based bipolar neutrosophic cross entropy measure for identification of rotor defects

Chander Parkash (C.P. Gandhi[1]), Jiawei Xiang[2]*, Anil Kumar[2], Govind Vashishtha[3], Ravi Kant[4],
[1]Department of Mathematics, Rayat Bahra University, Mohali, 140 104, India.
[2]College of Mechanical and Electrical Engineering, Wenzhou University, 325 035, China.
[3]Sant Longowal Institute of Engineering and Technology Longowal, 148 106, India
[4]Department of Electronics and Communications, Shoolini University, Solan (H.P.) India.
* Corresponding author, Email: wxw8627@163.com

Abstract

This study propounds a novel methodology for automatic identification of rotor defects severity, when the machine is operated at constant speed, through maximal overlap discrete wavelet packet transforms (MODWPT) and proposed cross entropy measures of bipolar neutrosophic sets, single valued neutrosophic sets and fuzzy sets respectively. After the 3rd level of decomposition of raw vibration signals into eight frequency bands (called as **WPT3** bands) through MODWPT, the energy reading in each **WPT3** band is monitored. Thereafter, the lower (here called as truth membership degrees) and upper energy bounds from the training and testing samples of various rotor defect conditions at each **WPT3** band are extracted and then normalized to lie in [0,1]. Finally, the energy intervals are constructed and thereafter converted into the desired forms of fuzzy sets, bipolar neutrosophic sets and single valued neutrosophic sets consecutively. The minimum cross entropy measure values between the fuzzy sets (**Method 1**), single valued neutrosophic sets (**Method 2)** and bipolar neutrosophic sets (**Method 3)** of training and testing samples of rotor defect conditions are computed and utilized to identify defect conditions such as angular/parallel misalignment of 10 Mils, unbalance, rub and defect free respectively. The novelty of the proposed rotor defect identification methodology lies in the fact that all the proposed variants of bipolar neutrosophic cross entropy measure have been found skilled enough to identify the desired rotor defects under study. On another hand, the existing cosine similarity measure [1] does not possess the necessary capability of identifying all rotor defects, especially, the rub defect condition. Furthermore, like the existing cosine similarity measure, our proposed variants of bipolar neutrosophic cross entropy measures have been found equally compatible for fairly furnishing the consistent and feasible results under intuitive analysis.

Keywords: Fuzzy Sets, Bipolar and Neutrosophic Sets, Cross Entropy, MODWPT, Rotor defects. Intuitive Analysis.

1. Introduction.

Rotating machinery is one of the critical element of any process industry[2]. Rotor is an integral part of any rotating machinery which helps in transmitting power from one component to another component. Rotors are generally subjected to experience shear stress due to various loading conditions and may lead to misalignment caused by the high torque,

resulted during the starting phase. The time and temperature-dependent property, known as creep, is also responsible for misaligning the rotor element. The misalignment leads to wearing of rotating components and power losses. The failure of highly integrated rotor element can invite several consequences and hence its continuous monitoring for engineering applications is essential [3]. The acquisition of vibration signals is crucial for condition monitoring as they may hide the critical information of rotor faults [4,5]. The information obtained by the misalignment condition of rotor element may provide knowledge about sub-harmonics and super-harmonics along with the shaft frequency, needed for various vibration responses [6].

A variety of rotor defect identification techniques have been developed and elaborated by eminent researchers in the current scenario. Kumar et al.[7] developed a new health indicator for the purpose of identifying some rotor defects after extracting successfully a total of 38 features from different domains which were further reduced to six features by the feature-based selection algorithm. Thereafter, manifold learning was effectively applied for fusing these six features, intended to develop novel indicators and identify angular and parallel misalignment conditions of the rotor. Darpe and Patel [8] explained the misalignment dynamics of the rotor through experimental investigations and reduced the ambiguity arises during the process of diagnosis. With the aid of full spectra, the authors have successfully denoised the misalignment after separating the faults having similar frequency spectrum. Shekhar and Prabhu[9] simulated the rotor-bearing system through Finite Element Analysis (FEM) by considering some essential influencing factors such as deflection, slope, shear, force and bending moment. In order to identify the misalignment of rotor, the authors have successfully evaluated the response to imbalance ratio up to two harmonics. Xiong et al.[10] excellently established a novel feature extraction method by combining the customized Hilbert-Huang Transform (HHT) with Kurtogram (also named as short time Fourier transform) for detecting and characterizing the fault information, hidden in the signals of a rotor-bearing assembly of the turbo-compressor machine set. Mereles and Cavalca [11] demonstrated a distributed parameter approach based upon the eigenfunctions of vibration signals and modeled a complex rotor-bearing system for the identification of rotor defects.

Xunshi et al. [12] introduced an end-to-end learning based fault identification procedure for collecting fusion information of multi-sensors in active magnetic bearing of

rotor system. Srinivas et al. [13] developed a least-square linear regression based technique for identifying misalignment and unbalance defect conditions in coupled rotor system, simulated by two-node Timoshenko beam finite element. Saavedra and Ramirez [14,15] carried out experimental investigations on a coupled rotor system, intended to identify the misalignment induced by coupling stiffness and load transmitted through the coupling. Bouyer and Fillon [16] experimentally demonstrated that misalignment in the rotor bearing system can be reduced through hydrodynamic effects. Chandra and Sekhar [17] used different time-frequency on run-up data of coupled rotor and identified the variation caused by angular and parallel misalignments in the system. Sinha [18] followed the concepts of bi-spectrum and tri-spectrum and detected both crack and misalignment defect conditions in a rotor test rig. Based on Lur'e description formulation, Gerami et al. [19] carried out a rocking beam experiment and discussed the advantages of designing a controller. The findings of the proposed controller clarified that the active magnetic bearing system could operate reliably under external and nonlinear disturbances and higher load capacity.

Xu et al. [20] combined the power spectral density of the vibration signals with the moving average cross-correlation coefficient for the purpose of developing a novel health indicator to track the health condition, estimate the remaining useful life and discriminate between different health states of bearings. Wang et al. [21] developed Shannon entropy and morphological transformation based fault identification methodology to confirm the influencing parameters of cyclo-stationary blind deconvolution [CYCBD}. Thereafter, the authors identified the highly sensitive component needed for amplifying the envelope spectrum of CYCBD signals. To detect electrical and mechanical faults of the winding of transformers, Abbasi et al. [22] combined the time series analysis approach with frequency response analysis in order to enhance the detection accuracy of the proposed method. Xiao et al. [23] modified the existing fast spectral correlation algorithm for analyzing raw vibration signals, generated some cyclic spectral correlation images, thereafter located the faulty frequency band and finally, with the help of square enhanced envelope spectrum, identified the fault type of rolling element bearing. Zhao et al. [24] formulated a cyclic correntropy (CCE) function in order to suppress the impulsive noises caused by rolling element bearing. Thereafter, the authors utilized the proclaimed CCE function to extract the kurtosis vectors required for training the LSSVM (least square support vector machine) for the purpose of identifying faults. Abbasi and Mahmoudi [25] discovered a new

methodology based on X-bar chart, R-chart, S-chart and frequency response analysis and utilized it to identify winding defects of transformers. Wodecki et al. [26] established a new methodology for local damage identification in bearings in the presence of non-cyclic and fault related cyclic impulses. By using alpha maximization criterion and feature optimization-gram, Mauricio et al. [27] developed an automated fault identification procedure to detect rolling element bearing defects in the presence of impulsive inferences such as Electromagnetic interference, impulsive noises and non-Gaussian noises. The authors successfully identified the inner race and outer race faults of the planet gear bearing in the rotatory machinery.

The afore-mentioned reported studies on rotor defect identification are mainly dealt with their experimental investigations and theoretical aspects, but with a lack of viewpoints from Information Theory prospective. One of the major challenges in tackling rotor defect identification methodologies is the gap between these methodologies and fuzzy and non-fuzzy measures of information. For this gap to be bridged, many variants of Shannon's information entropy have been made available to promote fault identification methodologies and classification accuracy of rotor defect conditions. Recently, Martinez et al. [28] used Shannon's entropy to quantify the amount of fault information hidden in the vibration signals of broken bars of induction motors. To describe the time-varied irregularities and complexities in the deterministic and stochastic power signals, Fu et al.[29] proposed an accurate and effective fast defect detection procedure based on the approximate entropy and wavelet transforms. Zhao et al. [30] developed a sensor fault diagnosis technique using wavelet entropy for analyzing the extracted sensor signals. The authors have excellently extracted the sensor fault information of a gas turbine by using instantaneous wavelet, singular and energy entropies. Leite et al [31] deployed the most fascinating Shannon's non-parametric measure as well as Renyi's parametric entropy measure for extracting the probability mass function (PMF) required for the characterization of bearing vibrations of a familiar time waveform. Zhang et al [32] employed Shannon's information entropy for reflecting the non-uniformity and irregularity of the decomposed vibrational response signal and identified the tightness degree of a bolt-jointed rotor. Zheng et al.[33] extended Shannon's entropy to a refined multiscale dispersion entropy for analyzing the vibration signals of defective rolling bearings and achieved the classification accuracy rate up to 100%. For early prognosis of bearing fault, Haidong et al.[34] integrated enhanced deep

GRU (gated recurrent unit) and wavelet entropy and applied it for studying the experimental and stimulated signals of rolling bearing. Continuous efforts have been made for developing fuzzy cross-entropy measure and signal processing technique-based fault identification methodologies for the enhancement of classification accuracy of rotor defects. Kumar et al.[35] established a novel fuzzy cross entropy loss function, hinged on the fuzzy sets of activation values and average activations value of the hidden layers of convolution neural network (CNN) and finally reduced the training parameters and avoided the over fitting of CNN. In another study, Kumar et al.[36] combined 3-level WPT with the proclaimed symmetric cross entropy measure, hinged on neutrosophic sets of training and testing samples of fault conditions, and successfully enhanced classification accuracy of rotor defect conditions. Kumar et al.[37] rehabilitated the vibration signals of training and testing samples of bearing defect conditions into the forms of fuzzy as well as neutrosophic sets and deployed the proffered variational mode decomposition and symmetric neutrosophic cross entropy measure based methodology to identify rotor defects in a centrifugal pump. Kumar et al.[38] established a novel neutrosophic entropy based frequency band selection methodology for identifying the most sensitive VMD frequency band (mode), intended to identify the desired defective component of an axial piston pump. Afia et al. [39] combined MODWPT, Shannon's entropy and MLPNN (multilayer perceptron neural network) for the purpose of automatically identification and classification of various types of gear defects under varying working conditions. Mauricio and Gryllias [40] established a novel disbound identification methodology based upon MODWPT and utilized it for extracting informative features, enhancing imaging efficiency and improving disbound identification accuracy of a composite material. Wang et al. [41] combined MODWPT with symplectic GMD(geometric mode decomposition) and multiscale DE (dispersion entropy) to decompose the original signals into symplectic GCs (geometric components) and effectively identified the most influencing frequency band responsible for defective components and thereafter removed some insignificant geometric components in a gear box. The reported studies on entropy-based fault identification methodologies have been mainly established by combining Shannon entropy with the enduring signal processing techniques including wavelet packet transforms, back propagation neural network, support vector machine, linear discrimination analysis, improved RBFNN etc. But many times, these entropy-based fault identification techniques have been found insufficient in providing semantic output due to

the difficulty in the decomposed signals, and revealing fault features of the noisy data under time varying conditions. One of the major draw backs in employing Shannon's entropy is its fancy assumption of 0log0=0, which hinders its applicability in tackling real engineering problems. Correspondingly, the first non-additive fuzzy cross entropy measure was elaborated by Bhandari and Pal [36]. Unfortunately, this infatuated cross entropy measure is facing some unavoidable drawbacks. Firstly, this is not symmetric in nature which creates a problematic situation for its usability in classifying the desired rotor defect conditions. Secondly, it produces inconsequential and unspecific results under certain mathematical treatments, especially, when its membership function conceives either zero or unity value. Furthermore, this asymmetrical fuzzy cross measure does not have the necessity capability to perform under intuitive analysis when tackling with noisy vibrational signals. The above-mentioned shortcomings/limitations have motivated the authors to develop the proposed bipolar neutrosophic cross entropy and MODWPT based rotor defect identification methodology. The proclaimed MODWPT and cross entropy-based approach may be quite complicated in the beginning, but it becomes interesting with the subsequent development of the proposed work. However, the proposed rotor defect identification methodology is applicable for automatic assessment of defect severities when the machine is operated at constant speed. The proposed variants of bipolar neutrosophic cross entropy measure have been successfully deployed for identifying various rotor defect conditions such as rub, unbalance, angular and parallel misalignment of 10 Mils, and defect free respectively. On another hand, the existing cosine similarity measure [42] based upon bipolar neutrosophic sets (BNSs) does not possess the necessary capability of identifying all rotor defects under study, especially, the rub defect condition. Furthermore, like the existing cosine similarity measure, our proposed variants of bipolar neutrosophic cross entropy measures are equally compatible for further mathematical treatments under intuitive environment.

After reviewing the existing literature on the proposed methodology, the overall technical gaps as observed can be outlined as below.

- The existing entropy-based fault identification methodologies have been mainly established by combining Shannon entropy with the enduring signal processing techniques. But many times, these techniques have been found insufficient in providing reliable output due to the fancy assumption of 0log0=0 in Shannon's

entropy. This hinders its usage in tackling rotor defect dentification problems.

- However, the first non-additive fuzzy cross entropy measure was elaborated by Bhandari and Pal [36]. Unfortunately, this infatuated cross entropy measure is also facing some unavoidable drawbacks such as this is not symmetric in nature. This creates a problematic situation for its usability in designing a reliable rotor defect identification methodology.
- Moreover, the existing fuzzy cross entropy may produce inconsequential and unspecific results under certain mathematical treatments, especially, when its membership function conceives either zero or unity value.
- The asymmetrical fuzzy cross measures do not have the necessity capability to perform under intuitive analysis when tackling with noisy vibrational signals. The above-mentioned shortcomings/limitations have motivated the authors to develop the proposed bipolar neutrosophic cross entropy and MODWPT based rotor defect identification methodology.
- The reported studies on rotor defect identification methodologies mainly deal with the experimental investigations and theoretical aspects, but with a lack of viewpoints from Information Theory prospective.

To bridge the gap between rotor defect identification methodologies and existing asymmetrical fuzzy cross entropy measures, many new variants of symmetrical fuzzy cross entropy measures have been developed and utilized to identify the desired rotor defect conditions such as angular/parallel misalignment of 10 Mils, unbalance, rub and defect free respectively.

The major contributions devoted to the study can be summarized as below.

- Establishment of a novel bipolar neutrosophic cross entropy and MODWPT based fault identification methodology.
- Owing to the incapability of existing cosine similarity measure [1] based on BNSs ,the proposed variants of bipolar neutrosophic cross entropy measure are intelligent in identifying various rotor defect conditions such as rub, unbalance, angular and parallel misalignment of 10 Mils, and defect free respectively.
- In this study, three different variants of bipolar neutrosophic cross entropy measures have been proposed. All these variants have been found capable in providing

remarkable fault information for various rotor defect conditions under study.

- All the proposed variants of bipolar neutrosophic cross entropy measures have been found skilled enough in providing consistent and feasible results under intuitive analysis.
- The proposed bipolar cross entropy and MODWPT-based methodology can efficiently identify bearing defects conditions when the machine is operated at constant speed. It can be extended to promote those rotor defect identification methodologies which can identify the bearing defects conditions when the machine is operated under varying speed and different load conditions.

The residuum of this underlying study is superseded as below.

Section 2 provides the brief introduction related to some familiar apprehensions on bipolar fuzzy sets (BFSs), single valued neutrosophic sets (SVNSs), bipolar neutrosophic sets (BNSs) and their cross-entropy measures. **Section 3** validates the construction of a novel symmetric fuzzy cross entropy measure hinged on two fuzzy sets. **Sections 4-5** extend the outcomes of **Section 3** to construct another novel cross entropy measures hinged on two SVNSs and BNSs consecutively. To identify various rotor defect conditions, a novel bipolar neutrosophic cross entropy and MODWPT based methodology is developed in **Section 6.** In **Section 7,** the proposed variants of bipolar neutrosophic cross entropy measures are efficiently deployed for identifying various rotor defect conditions such as angular and parallel misalignment of 10 mils, rub, unbalance and defect free. The concrete conclusion of the underlying study is provided in **Section 8.**

2. Preliminaries: -

A fuzzy cross entropy measure is hinged on two fuzzy sets [36] and can be extended to this measure hinged on two single valued neutrosophic sets [36,37,42] and bipolar single valued neutrosophic set. A bipolar fuzzy set [1] is an advance version of the fuzzy set and can be extended to bipolar neutrosophic set which can reveal more fault information when deployed for identifying rotor defect conditions under study.

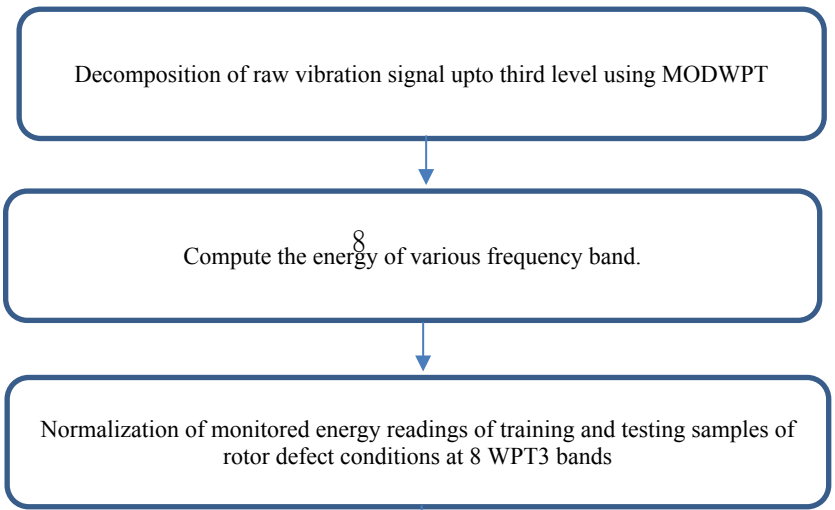

Fig.1 A schematic diagram of bipolar neutrosophic cross entropy and MODWPT based methodology for identifying rotor defect conditions

Def. 2.1 Fuzzy Set: Let X be any finite discourse of universe generated by generic elements $x_1,x_2,...x_n$. A fuzzy set (FS), denoted as $\tilde{A}_{FS} \subseteq X$,is an object of the form: $\tilde{A}_{FS} = \{ < x_i,\tilde{\mu}_{A^f}(x_i) > | x_i \in X, i = 1,2,...,n\}$, characterized by membership function $\tilde{\mu}_{A^f}(x_i)$:$X \rightarrow [0,1]$ where $\tilde{\mu}_{A^f}(x_i)$ represents the grade or degree of truth membership of an i^{th} generic element in X and satisfy $0 \leq \tilde{\mu}_{A^f}(x_i) \leq 1$. Also, the complement $C(\tilde{A}_{FS})$ is defined as $C(\tilde{A}_{FS}) = \{ < x_i,1 - \tilde{\mu}_{A^f}(x_i) > | x_i \in X, i = 1,2,...,n\}$.

Def. 2.2 Bipolar Fuzzy Set [1]**:**A bipolar fuzzy set (BFS), denoted as $\tilde{A}^b_{FS} \subseteq X$, is a hybrid combination of positive membership function $\tilde{\mu}^+_{A^f}(x)$:$X \rightarrow [0,1]$ and negative membership

function $\tilde{\mu}_{A^f}^{-}(x)$:$X\rightarrow[-1,0]$. Thus,$\tilde{A}_{FS}^{b}=\{<x_i,\tilde{\mu}_{A^f}^{+}(x_i),\tilde{\mu}_{A^f}^{-}(x_i)>|x_i\in X,i\in N\}$ where $0\leq\tilde{\mu}_{A^f}^{+}(x_i)\leq 1$ and $-1\leq\tilde{\mu}_{A^f}^{-}(x_i)\leq 0\forall i=1,2,...,n$. Further, the complement $C(\tilde{A}_{FS}^{b})$ of a bipolar fuzzy set $\tilde{A}_{FS}^{b}\subseteq X$ is defined as $C(\tilde{A}_{FS}^{b})=\{<x_i,1-\tilde{\mu}_{A^f}^{+}(x_i),-1-\tilde{\mu}_{A^f}^{-}(x)>|x_i\in X,i\in N\}$.

Def. 2.3 Single Valued Neutrosophic Set [36,37]**:** It is an object of the form: $\tilde{A}_{SV}^{n}=\{<x_i,\tilde{\mu}_{A^f}(x_i),\tilde{i}_{A^f}(x_i),\tilde{f}_{A^f}(x_i)>|x_i\in X\};\tilde{\mu}_{A^f}(x_i),\tilde{i}_{A^f}(x_i),\tilde{f}_{A^f}(x_i)$:$X\rightarrow[0,1]$ where each $\tilde{\mu}_{A^f}(x_i),\tilde{i}_{A^f}(x_i),\tilde{f}_{A^f}(x_i)$ represent grade or degree of truth membership, indeterminacy membership and falsity membership respectively and satisfy $0\leq\tilde{\mu}_{A^f}(x_i)+\tilde{i}_{A^f}(x_i)+\tilde{f}_{A^f}(x_i)\leq 3$. Also, the complement $C(\tilde{A}_{SV}^{n})$ is defined as $C(\tilde{A}_{SV}^{n})=\{<x_i,\tilde{f}_{A^f}(x_i),1-\tilde{i}_{A^f}(x_i),\tilde{\mu}_{A^f}(x_i)>|x_i\in X\}$.

Def. 2.4 Bipolar Neutrosophic Set [1]**:**It is a hybrid combination of two independent parts: $\tilde{\mu}_{A^f}^{+}(x_i),\tilde{i}_{A^f}^{+}(x_i),\tilde{f}_{A^f}^{+}(x_i)$:$X\rightarrow[0,1]$; $\tilde{\mu}_{A^f}^{-}(x_i),\tilde{i}_{A^f}^{-}(x_i),\tilde{f}_{A^f}^{-}(x_i)$:$X\rightarrow[-1,0]$ where each $\tilde{\mu}_{A^f}^{+}(x_i),\tilde{i}_{A^f}^{+}(x_i),\tilde{f}_{A^f}^{+}(x_i)$ denote positive grade or degree of truth membership, indeterminate membership and falsity membership of the generic element $x_i\in X$. Similarly, $\tilde{\mu}_{A^f}^{-}(x_i),\tilde{i}_{A^f}^{-}(x_i),\tilde{f}_{A^f}^{-}(x_i)$ represent negative grade or degree of truth membership, indeterminate membership and falsity membership of $x_i\in X$ representing some implicit property countered by $\tilde{A}_{\mathrm{BP}}^{n}\subseteq X$. It is defined as

$\tilde{A}_{BP}^{n}=\{<x_i,\tilde{\mu}_{A^f}^{+}(x_i),\tilde{i}_{A^f}^{+}(x_i),\tilde{f}_{A^f}^{+}(x_i),\tilde{\mu}_{A^f}^{-}(x_i),\tilde{i}_{A^f}^{-}(x_i),\tilde{f}_{A^f}^{-}(x_i)>|x_i\in X,i\varepsilon N\}$such that $0\leq\tilde{\mu}_{A^f}^{+}(x)+\tilde{i}_{A^f}^{+}(x)+\tilde{f}_{A^f}^{+}(x)\leq 3;-3\leq\tilde{\mu}_{A^f}^{-}(x)+\tilde{i}_{A^f}^{-}(x)+\tilde{f}_{A^f}^{-}(x)\leq 0$.

Also, the complement $C(\tilde{A}_{\mathrm{BP}}^{n})$is defined as

$$C(\tilde{A}_{BP}^{n})=\{<x_i,1-\tilde{\mu}_{A^f}^{+}(x_i),1-\tilde{i}_{A^f}^{+}(x_i),1-\tilde{f}_{A^f}^{+}(x_i),-1-\tilde{\mu}_{A^f}^{-}(x_i),-1-\tilde{i}_{A^f}^{-}(x_i),-1-\tilde{f}_{A^f}^{-}(x_i)>|x_i\in X\}$$

Def. 2.5 Symmetric Fuzzy Cross Entropy Measure [36]**:**Suppose $F(X)$denotes the collection of all fuzzy sets. Let $\tilde{A}_{FS}=\{<x_i,\tilde{\mu}_{A^f}(x_i)>|x_i\in X\}\in F(X)$ and $\tilde{B}_{FS}=\{<x_i,\tilde{\mu}_{B^f}(x_i)>|x_i\in X\}\in F(X)$be any two fuzzy sets in $F(X)$. Then a function H_{CE}:$F(X)\times F(X)\rightarrow R^{+}$ (the set of non-negative reals) is named as symmetric fuzzy cross entropy measure hinged on $\tilde{A}_{FS}$ and $\tilde{B}_{FS}$ if $(i)H_{CE}(\tilde{A}_{FS},\tilde{B}_{FS})\geq 0(ii)H_{CE}(\tilde{A}_{FS},\tilde{B}_{FS})=0$ if and only if $\tilde{A}_{FS}=\tilde{B}_{FS}$. $(iii)H_{CE}(\tilde{A}_{FS},\tilde{B}_{FS})=H_{CE}(\tilde{B}_{FS},\tilde{A}_{FS})\forall\tilde{A}_{FS},\tilde{B}_{FS}\in F(X)$. $(iv)H_{CE}(C(\tilde{A}_{FS}),C(\tilde{B}_{FS}))=H_{CE}(\tilde{A}_{FS},\tilde{B}_{FS})\forall\tilde{A}_{FS},\tilde{B}_{FS}\in F(X)$.

Def. 2.6 Symmetric Neutrosophic Cross Entropy Measure [37]**:**Suppose $S(X)$denotes the collection of all single valued neutrosophic sets (SVNSs) and $\tilde{A}_{SV}^{n}=\{<x_i,\tilde{\mu}_{A^f}(x_i),\tilde{i}_{A^f}(x_i),\tilde{f}_{A^f}(x_i)>|x_i\in X\}\in S(X)$; $B_{SV}^{n}=$

$\{< x_i,\tilde{\mu}_{B^f}(x_i),\tilde{i}_{B^f}(x_i),\tilde{f}_{B^f}(x_i) > |x_i \in X\} \in S(X)$.Then a function S_{CE}:$S(X) \times S(X) \rightarrow R^+$ is called as symmetric single valued neutrosophic cross entropy measure hinged on two SVNSs $\tilde{A}^n_{SV}$ and $\tilde{B}^n_{SV}$if

$(i) S_{CE}(\tilde{A}^n_{SV},\tilde{B}^n_{SV}) \geq 0 (ii) S_{CE}(\tilde{A}^n_{SV},\tilde{B}^n_{SV}) = 0$ if and only if $\tilde{A}^n_{SV} = \tilde{B}^n_{SV}$. $(iii) S_{CE}(\tilde{A}^n_{SV},\tilde{B}^n_{SV}) = S_{CE}(\tilde{B}^n_{SV},\tilde{A}^n_{SV}) \forall \tilde{A}^n_{SV},\tilde{B}^n_{SV} \in S(X)$.

$(iv) S_{CE}(C(\tilde{A}^n_{SV}),C(\tilde{B}^n_{SV})) = S_{CE}(\tilde{A}^n_{SV},\tilde{B}^n_{SV}) \forall \tilde{A}^n_{SV},\tilde{B}^n_{SV} \in S(X)$.

Def. 2.7 Bipolar Neutrosophic Cross Entropy Measure: Let$B(X)$denotes the collection of all bipolar neutrosophic sets (BNSs). Let

$\tilde{A}^n_{BP} = \{< x_i,\tilde{\mu}^+_{A^f}(x_i),\tilde{i}^+_{A^f}(x_i),\tilde{f}^+_{A^f}(x_i),\tilde{\mu}^-_{A^f}(x_i),\tilde{i}^-_{A^f}(x_i),\tilde{f}^-_{A^f}(x_i) > |x_i \in X, i = 1,2,...,n\} \in B(X)$

and

$\tilde{B}^n_{BP} = \{< x_i,\tilde{\mu}^+_{B^f}(x_i),\tilde{i}^+_{B^f}(x_i),\tilde{f}^+_{B^f}(x_i),\tilde{\mu}^-_{B^f}(x_i),\tilde{i}^-_{B^f}(x_i),\tilde{f}^-_{B^f}(x_i) > |x_i \in X, i = 1,2,...,n\} \in B(X)$

be any two BNSs. A function P_{CE}:$B(X) \times B(X) \rightarrow R^+$ is called a symmetric bipolar neutrosophic cross entropy measure if

$(i) P_{CE}(\tilde{A}^n_{BP},\tilde{B}^n_{BP}) \geq 0 \forall \tilde{A}^n_{BP},\tilde{B}^n_{BP} \in B(X)$ $(ii) P_{CE}(\tilde{A}^n_{BP},\tilde{B}^n_{BP}) = 0$ if $\tilde{A}^n_{BP} = \tilde{B}^n_{BP}$. (iii)$S_{CE}$ $(\tilde{A}^n_{BP},\tilde{B}^n_{BP}) = S_{CE}(\tilde{B}^n_{BP},\tilde{A}^n_{BP}) \forall \tilde{A}^n_{BP},\tilde{B}^n_{BP} \in B(X)$.

$(iv) S_{CE}(C(\tilde{A}^n_{BP}),C(\tilde{B}^n_{BP})) = S_{CE}(\tilde{A}^n_{BP},\tilde{B}^n_{BP}) \forall \tilde{A}^n_{BP},\tilde{B}^n_{BP} \in B(X)$.

3. A SYMMETRIC FUZZYCROSS ENTROPY MEASURE

The establishment of the following **Theorem 3.1** shall play a vital role in the construction of novel symmetric single valued neutrosophic cross entropy measure (**Section 4),** the outcomings of which shall be utilized for constructing another novel bipolar neutrosophic cross entropy measure (**Section 5)**.

Theorem.3.1 If we set $R_0 = \tilde{\mu}_{A^f}(x_i) + \tilde{\mu}_{B^f}(x_i)$, $R_1 = \sqrt{\tilde{\mu}_{A^f}(x_i)} + \sqrt{\tilde{\mu}_{B^f}(x_i)}$ and $R_2 = \sqrt{1 - \tilde{\mu}_{A^f}(x_i)} + \sqrt{1 - \tilde{\mu}_{B^f}(x_i)}$, then $H^{\mu}_{CE}(\tilde{A}_{FS},\tilde{B}_{FS})$ is a correct symmetric inverse hyperbolic fuzzy cross entropy measure hinged on fuzzy sets $\tilde{A}_{FS}$ and $\tilde{B}_{FS}$ where

$H^{\mu}_{CE}(\tilde{A}_{FS},\tilde{B}_{FS}) =$

$$\sum_{i=1}^{n}\left[-8tanh^{-1}\frac{1}{2} + (3 + R_0)tanh^{-1}\left(\frac{1 + R_0^2 + R_1^2}{2 + (2 + R_0)R_1^2}\right) + (5 - R_0)tanh^{-1}\left(\frac{1 + (2 - R_0)^2 + R_2^2}{2 + (4 - R_0)R_2^2}\right)\right] \quad \ldots (1)$$

Here, $H^{\mu}_{CE}(\tilde{A}_{FS},\tilde{B}_{FS})$ indicates the amount of fuzziness due to truth membership degree of symmetric discrimination of the fuzzy set $\tilde{A}_{FS}$ against $\tilde{B}_{FS}$.

Proof. The proposed fuzzy cross entropy measure $H^{\mu}_{CE}(\tilde{A}_{FS},\tilde{B}_{FS})$ satisfies the essential conditions (ii) and (iii) of **Def. 2.5.** To establish the non-negativity of $H^{\mu}_{CE}(\tilde{A}_{FS},\tilde{B}_{FS})$, we shall first establish the **Lemma 3.1.**

Lemma 3.1 Let $\tilde{A}_{FS} = \{ < x_i, \tilde{\mu}_{A^f}(x_i) > | x_i \in X\}$ & $\tilde{B}_{FS} = \{ < x_i, \tilde{\mu}_{B^f}(x_i) > | x_i \in X\}$be any two fuzzy sets. Define $Q(\tilde{\mu}_{A^f}(x_i), \tilde{\mu}_{B^f}(x_i)) = \frac{\tilde{\mu}_{A^f}(x_i) + \tilde{\mu}_{B^f}(x_i)}{2}$,$P(\tilde{\mu}_{A^f}(x_i), \tilde{\mu}_{B^f}(x_i)) = \left(\frac{\tilde{\mu}_{A^f}(x_i) + \tilde{\mu}_{B^f}(x_i)}{\sqrt{\tilde{\mu}_{A^f}(x_i)} + \sqrt{\tilde{\mu}_{B^f}(x_i)}}\right)^2$. Then there exists the inequality:

$$P(\tilde{\mu}_{A^f}(x_i), \tilde{\mu}_{B^f}(x_i)) \geq Q(\tilde{\mu}_{A^f}(x_i), \tilde{\mu}_{B^f}(x_i)) \quad \ldots (2)$$

with equality if and only if $\tilde{\mu}_{A^f}(x_i) = \tilde{\mu}_{B^f}(x_i)$.

Proof. The resulting inequality **(2)** shall be true if **(3)** holds. Thus,

$$\left(\frac{\tilde{\mu}_{A^f}(x_i) + \tilde{\mu}_{B^f}(x_i)}{\sqrt{\tilde{\mu}_{A^f}(x_i)} + \sqrt{\tilde{\mu}_{B^f}(x_i)}}\right)^2 \geq \frac{\tilde{\mu}_{A^f}(x_i) + \tilde{\mu}_{B^f}(x_i)}{2} \quad \ldots (3)$$

$$\Leftrightarrow 2(\tilde{\mu}_{A^f}(x_i) + \tilde{\mu}_{B^f}(x_i)) \geq \left(\sqrt{\tilde{\mu}_{A^f}(x_i)} + \sqrt{\tilde{\mu}_{B^f}(x_i)}\right)^2$$

$$\Leftrightarrow \tilde{\mu}_{A^f}(x_i) + \tilde{\mu}_{B^f}(x_i) - 2\sqrt{\tilde{\mu}_{A^f}(x_i)}\sqrt{\tilde{\mu}_{B^f}(x_i)} \geq 0$$

$$\Leftrightarrow \left(\sqrt{\tilde{\mu}_{A^f}(x_i)} - \sqrt{\tilde{\mu}_{B^f}(x_i)}\right)^2 \geq 0 \quad \ldots (4)$$

which is obviously true. Also, the equality occurs in **(4)** if and only if $\tilde{\mu}_{A^f}(x_i) = \tilde{\mu}_{B^f}(x_i)$. Thus, keeping in mind the resulting **Lemma 3.1** and our usual notations $Q = \frac{R_0}{2}$ *and* $P = \frac{R_0^2}{R_1^2}$. the forthcoming inequality **(2)** can be re-designed as

$$\frac{R_0^2}{R_1^2} \geq \frac{R_0}{2} \Rightarrow \frac{R_0^2}{R_1^2} + 1 \geq \frac{R_0}{2} + 1 \Rightarrow R_0^2 + R_1^2 \geq \frac{(2 + R_0)R_1^2}{2}$$

$$\Rightarrow R_0^2 + R_1^2 + 1 \geq \frac{(2 + R_0)R_1^2}{2} + 1 \Rightarrow \frac{1 + R_0^2 + R_1^2}{2 + (2 + R_0)R_1^2} \geq \frac{1}{2} \quad \ldots (5)$$

Since $tanh^{-1}$ exhibits its monotonicity over (0,1), the undergoing inequality **(5)** can be modified as

$$(3 + R_0) tanh^{-1}\left(\frac{1 + R_0^2 + R_1^2}{2 + (2 + R_0)R_1^2}\right) \geq (3 + R_0) tanh^{-1}\frac{1}{2} \quad \ldots (6)$$

Replacement of $\tilde{\mu}_{A^f}(x_i), \tilde{\mu}_{B^f}(x_i)$ with their counterparts $1 - \tilde{\mu}_{A^f}(x_i), 1 - \tilde{\mu}_{B^f}(x_i)$ in the undergoing inequality **(6)** yields

$$(5 - R_0) tanh^{-1}\left(\frac{1 + (2 - R_0)^2 + R_2^2}{2 + (4 - R_0)R_2^2}\right) \geq (5 - R_0) tanh^{-1}\frac{1}{2} \quad \ldots (7)$$

If we can simply add **(6)** & **(7)** and then take the sum ranging from $i = 1$ to n, then the desired result follows. Thus,$H_{CE}(\tilde{A}_{FS}, \tilde{B}_{FS}) \geq 0 \forall \tilde{A}_{FS}, \tilde{B}_{FS} \in F(X)$ with equality if and only if $\tilde{\mu}_{A^f}(x_i) = \tilde{\mu}_{B^f}(x_i)$. The fact that $H_{CE}^{\mu}(\tilde{A}_{FS}, \tilde{B}_{FS})$ admits its non-negative values can

also be experienced from the surface plot as shown in **Fig. 2(a, b).**

4. A SYMMETRIC NEUTROSOPHIC CROSS ENTROPY MEASURE

We shall now extend the outcomes of **Theorem 3.1** to develop another novel cross entropy measure hinged on two single valued neutrosophic sets as follows.

Def. 4.1 Let $\tilde{A}_{SV}^{n} = \{ < x_i, \tilde{\mu}_{A^f}(x_i), \tilde{i}_{A^f}(x_i), \tilde{f}_{A^f}(x_i) > | x_i \in X \} \in S(X)$and $\tilde{B}_{SV}^{n} = \{ < x_i, \tilde{\mu}_{B^f}(x_i), \tilde{i}_{B^f}(x_i), \tilde{f}_{B^f}(x_i) > | x_i \in X \} \in S(X)$be any single valued neutrosophic sets**.** In view of **Theorem 3.1,** the amount of fuzziness due to truth membership degree of symmetric discrimination of $\tilde{A}_{FS}$ against $\tilde{B}_{FS}$, represented by $H_{CE}^{\mu}(\tilde{A}_{FS}, \tilde{B}_{FS})$, has been established by equation **(1).** Set $S_0 = \tilde{i}_{A^f}(x_i) + \tilde{i}_{B^f}(x_i)$, $S_1 = \sqrt{\tilde{i}_{A^f}(x_i)} + \sqrt{\tilde{i}_{B^f}(x_i)}$and $S_2 = \sqrt{1 - \tilde{i}_{A^f}(x_i)} + \sqrt{1 - \tilde{i}_{B^f}(x_i)}$, $T_0 = \tilde{f}_{A^f}(x_i) + \tilde{f}_{B^f}(x_i)$ $T_1 = \sqrt{\tilde{f}_{A^f}(x_i)} + \sqrt{\tilde{f}_{B^f}(x_i)}$ and $T_2 = \sqrt{1 - \tilde{f}_{A^f}(x_i)} + \sqrt{1 - \tilde{f}_{B^f}(x_i)}$.Then, the amount of fuzziness due to indeterminacy membership degree, represented by $H_{CE}^{i}(\tilde{A}_{FS}, \tilde{B}_{FS})$, and falsity membership degree, represented by $H_{CE}^{f}(\tilde{A}_{FS}, \tilde{B}_{FS})$, of their symmetric discrimination of $\tilde{A}_{FS}$ against $\tilde{B}_{FS}$ can also be established employing **Theorem 3.1.** Thus

$$H_{CE}^{i}(\tilde{A}_{FS}, \tilde{B}_{FS}) = \sum_{i=1}^{n} \left[-8 tanh^{-1} \frac{1}{2} + (3 + S_0) tanh^{-1} \left(\frac{1 + S_0^2 + S_1^2}{2 + (2 + S_0) S_1^2} \right) + (5 - S_0) tanh^{-1} \left(\frac{1 + (2 - S_0)^2 + S_2^2}{2 + (4 - S_0) S_2^2} \right) \right] \quad \ldots (8)$$

$$H_{CE}^{f}(\tilde{A}_{FS}, \tilde{B}_{FS}) = \sum_{i=1}^{n} \left[-8 tanh^{-1} \frac{1}{2} + (3 + T_0) tanh^{-1} \left(\frac{1 + T_0^2 + T_1^2}{2 + (2 + T_0) T_1^2} \right) + (5 - T_0) tanh^{-1} \left(\frac{1 + (2 - T_0)^2 + T_2^2}{2 + (4 - T_0) T_2^2} \right) \right] \quad \ldots (9)$$

Hence, the desired symmetric single valued neutrosophic cross entropy measure, represented by $S_{CE}(\tilde{A}_{SV}^{n}, \tilde{B}_{SV}^{n})$, hinged on two single valued neutrosophic sets $\tilde{A}_{SV}^{n}$ and $\tilde{B}_{SV}^{n}$, can be easily obtained by simply adding the resulting equations **(1), (8)**

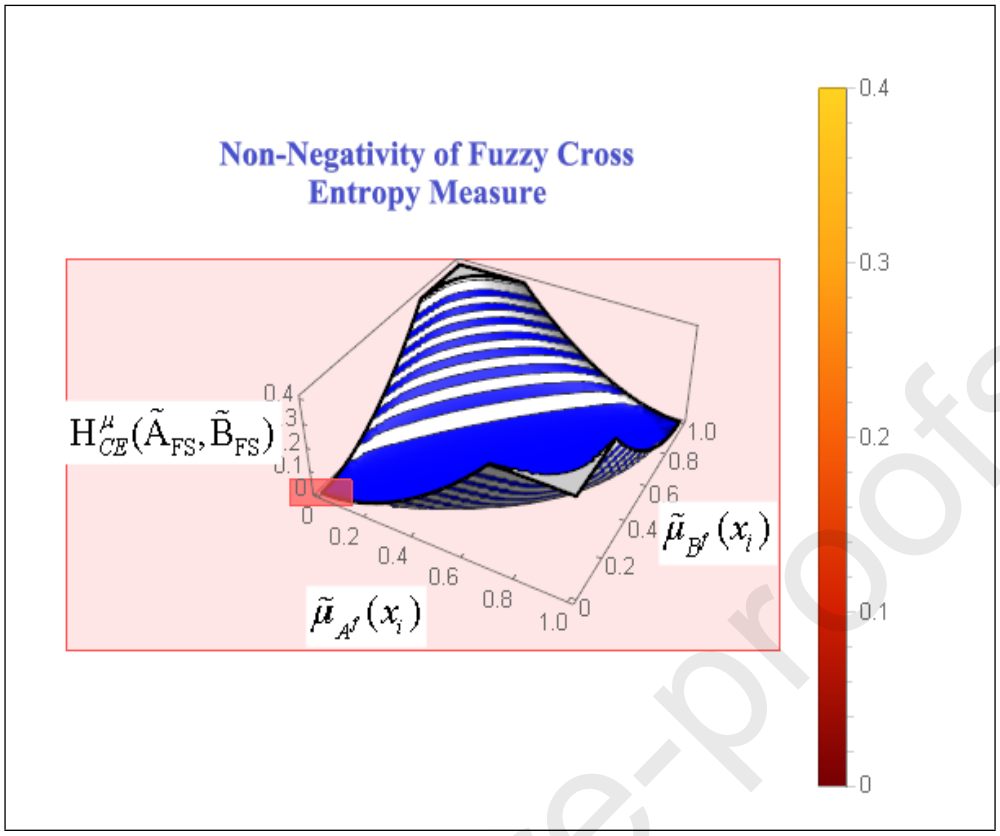

(a)

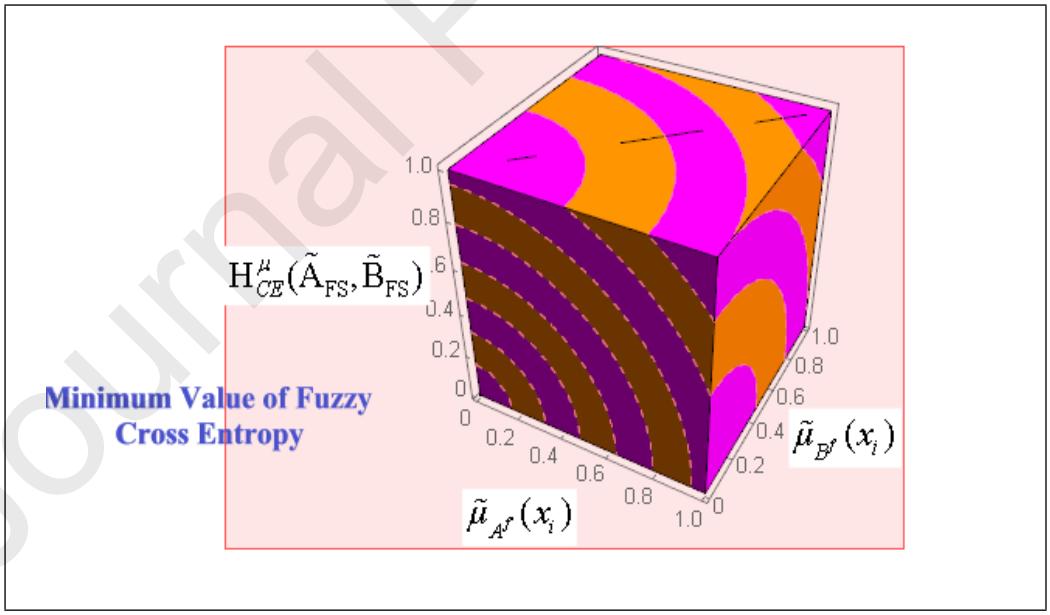

(b)

Fig.2 (a) Non negativity property and (b) Minimum value admitted by $H^{\mu}_{CE}(\tilde{A}_{FS},\tilde{B}_{FS})$.

and **(9)** as follows.

$$S_{CE}\left(\tilde{A}_{SV}^{n},\tilde{B}_{SV}^{n}\right) = H_{CE}^{\mu}(\tilde{A}_{FS},\tilde{B}_{FS})(Eq.1) + H_{CE}^{i}(\tilde{A}_{FS},\tilde{B}_{FS})(Eq.8) + H_{CE}^{f}(\tilde{A}_{FS},\tilde{B}_{FS})(Eq.9) \quad \ldots (10)$$

The neutrosophic cross entropy measure $S_{CE}\left(\tilde{A}_{SV}^{n},\tilde{B}_{SV}^{n}\right)$ indicates the amount of fuzziness due to symmetric discrimination of the single valued neutrosophic sets (SVNSs) $\tilde{A}_{SV}^{n}$ against $\tilde{B}_{SV}^{n}$. It is informative to indicate that the proclaimed cross entropy measure **(10)** hinged on two SVNSs can be further extended to this measure hinged on two bipolar neutrosophic sets as follows.

5. A BIPOLAR NEUTROSOPHIC CROSS ENTROPY MEASURE

The outcropped variants of cross entropy measures **(1), (8)** and **(9)** can be utilized to construct the proclaimed bipolar neutrosophic cross entropy measure as ventilated by **Theorem 5.1.**

Theorem.5.1 $T_{CE}\left(\tilde{A}_{BP}^{n},\tilde{B}_{BP}^{n}\right)$ is an authentic inverse hyperbolic symmetric bipolar neutrosophic cross entropy measure hinged on two bipolar neutrosophic sets $\tilde{A}_{BP}^{n}$ and $\tilde{B}_{BP}^{n}$ represented as

$$T_{CE}\left(\tilde{A}_{BP}^{n},\tilde{B}_{BP}^{n}\right) =$$

$$\sum_{i=1}^{n}\left[\begin{array}{l} -16tanh^{-1}\frac{1}{2} + (3+R_0^{+})tanh^{-1}\left(\frac{1+R_0^{+2}+R_1^{+2}}{2+(2+R_0^{+})R_1^{+2}}\right) + (5-R_0^{+})tanh^{-1}\left(\frac{1+(2-R_0^{+})^2+R_2^{+2}}{2+(4-R_0^{+})R_2^{+2}}\right) \\ \qquad + (3-R_0^{-})tanh^{-1}\left(\frac{1+R_0^{-2}+R_1^{-2}}{2+(2-R_0^{-})R_1^{-2}}\right) + (5+R_0^{-})tanh^{-1}\left(\frac{1+(2+R_0^{-})^2+R_2^{-2}}{2+(4+R_0^{-})R_2^{-2}}\right) \end{array}\right]$$

$$+$$

$$\sum_{i=1}^{n}\left[\begin{array}{l} -16tanh^{-1}\frac{1}{2} + (3+S_0^{+})tanh^{-1}\left(\frac{1+S_0^{+2}+S_1^{+2}}{2+(2+S_0^{+})S_1^{+2}}\right) + (5-S_0^{+})tanh^{-1}\left(\frac{1+(2-S_0^{+})^2+S_2^{+2}}{2+(4-S_0^{+})S_2^{+2}}\right) \\ \qquad + (3-S_0^{-})tanh^{-1}\left(\frac{1+S_0^{-2}+S_1^{-2}}{2+(2-S_0^{-})S_1^{-2}}\right) + (5+S_0^{-})tanh^{-1}\left(\frac{1+(2+S_0^{-})^2+S_2^{-2}}{2+(4+S_0^{-})S_2^{-2}}\right) \end{array}\right]$$

$$+$$

$$\sum_{i=1}^{n}\left[\begin{array}{l} -16tanh^{-1}\frac{1}{2} + (3+T_0^{+})tanh^{-1}\left(\frac{1+T_0^{+2}+T_1^{+2}}{2+(2+T_0^{+})T_1^{+2}}\right) + (5-T_0^{+})tanh^{-1}\left(\frac{1+(2-T_0^{+})^2+T_2^{+2}}{2+(4-T_0^{+})T_2^{+2}}\right) \\ \qquad + (3-T_0^{-})tanh^{-1}\left(\frac{1+T_0^{-2}+T_1^{-2}}{2+(2-T_0^{-})T_1^{-2}}\right) + (5+T_0^{-})tanh^{-1}\left(\frac{1+(2+T_0^{-})^2+T_2^{-2}}{2+(4+T_0^{-})T_2^{-2}}\right) \end{array}\right]$$

… (11)

The notations with their meanings are provided in APPENDIX-A.1. Here, $T_{CE}\left(\tilde{A}_{BP}^{n},\tilde{B}_{BP}^{n}\right)$

indicates the amount of fuzziness due to symmetric discrimination of the bipolar single valued neutrosophic set $\tilde{A}_{BP}^{n}$against $\tilde{B}_{BP}^{n}$.

Proof. The conditions (i), (ii), (iii) and (ii) of **Def. 2.7** are straightforward.

The overhead discussion has finally put us in a conclusive position to authenticate the applicability and effectiveness of the proposed variants of bipolar neutrosophic cross entropy measures represented by **(1), (10)** and **(11)** as follows.

6. Bipolar Neutrosophic Cross Entropy and MODWPT Based Methodology

In this section, our endeavor is to establish a novel rotor defect identification methodology by combining maximal overlap discrete wavelet packet transforms with the proposed variants of bipolar neutrosophic cross entropy measures, represented by **(1), (10)** and **(11)** as follows.

Step 1: - Data Acquisition

The study for rotor fault identification was carried out on the test bench shown in **Fig. 3.** The test bench consists of 3 phase induction motor which is connected to the rotor through coupling. The experiment was carried out at a fixed speed of 20 Hz. For acquisition of vibration data, tri-axial accelerometer was attached on the housing of bearing located at non-drive end. The vibration data acquired in vertical direction was used for the analysis. In this study, we have obtained various familiar rotor defect conditions and represented them by the set $B_K = (B_1, B_2, B_3, B_4, B_5)$ as depicted in **Table 1.**

Table 1: Description of various rotor defect conditions

Condition	**Description**
Defect free	B_1
Angular misalignment of 10 Mils	B_2
Parallel misalignment of 10 Mils	B_3
Rub	B_4

Unbalance	B_5

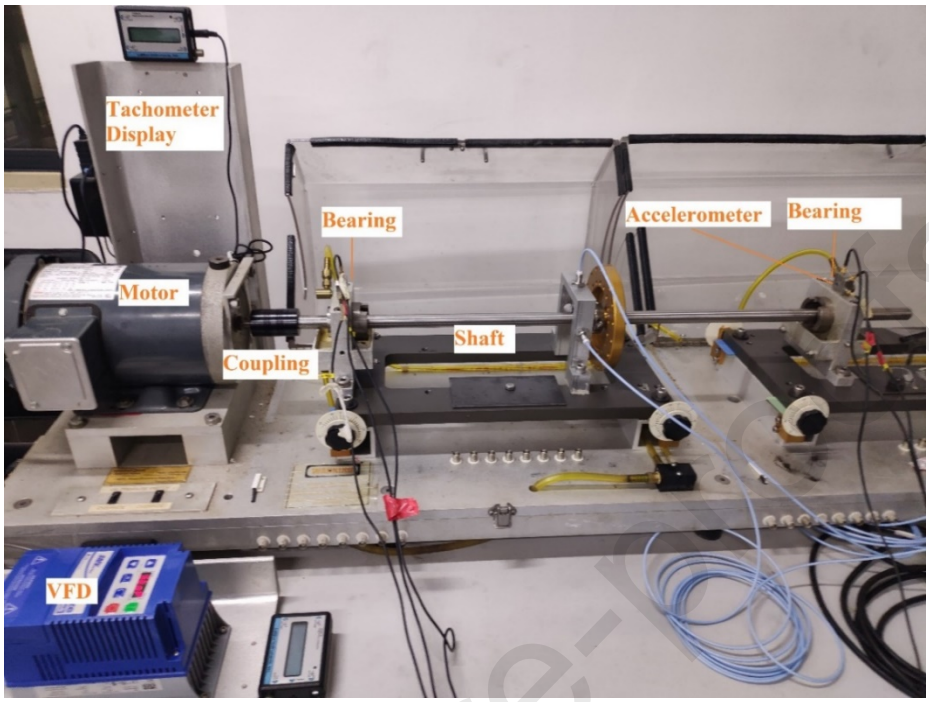

Fig. 3 Fault Simulator used for experimental investigations

Step 2: - Decomposition of Raw Signals Through MODWPT

Discrete wavelet transform is, however, a significant technique for data acquisition, but struggling with some technical issues like it is incapable for decomposing high frequency (detail) signals and does not possess the shift invariance property. Maximal overlap discrete wavelet packet transformation (MODWPT) possesses the shift invariance property and can decompose both high frequency (detail) and low frequency (approximate) signals in time frequency domain. This has motivated the authors to deploy MODWPT to decompose the raw vibration signals at three level of decomposition into 8 sub-frequency bands (called as **WPT3** bands). Let $W_{j,n}^{(M)} = \{W_{j,n,t}^{(M)}, t = 0,1,2,\ldots N_j - 1\}$ be the sequence of MODWPT coefficients at the j^{th} level and the frequency-index n. With $W_{0,0}^{(M)} = X$, and the series $\left\{W_{j-1,\frac{n}{2},t}^{(M)}\right\}$ of length N, then the coefficient $\{W_{j,n,t}^{(M)}\}$ can be obtained by using [43,44] and is given by **(12).**

$$W_{j,n,t}^{(M)} = \sum_{l=0}^{L-1} r_{n,l} W_{j-1,\left[\frac{n}{2}\right],(t-2^j l) mod\, N}^{(M)} \quad \ldots (12)$$

A typical signal resulted from defect free, angular misalignment of 10 Mils, parallel misalignment of 10 Mils, unbalance and rub defect conditions are depicted in **Fig 4(a)-8(a).**

The corresponding decomposed signals of these fault conditions into 8 **WPT3** bands have been obtained by deploying 3-level MODWPT **WPT3** bands and are depicted in **Fig 4(b)-8(b).** The computation time of MODWPT signal is almost 0.07 sec.

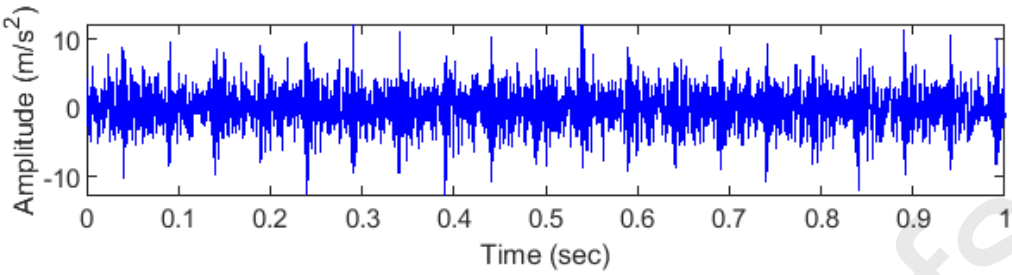

(a)

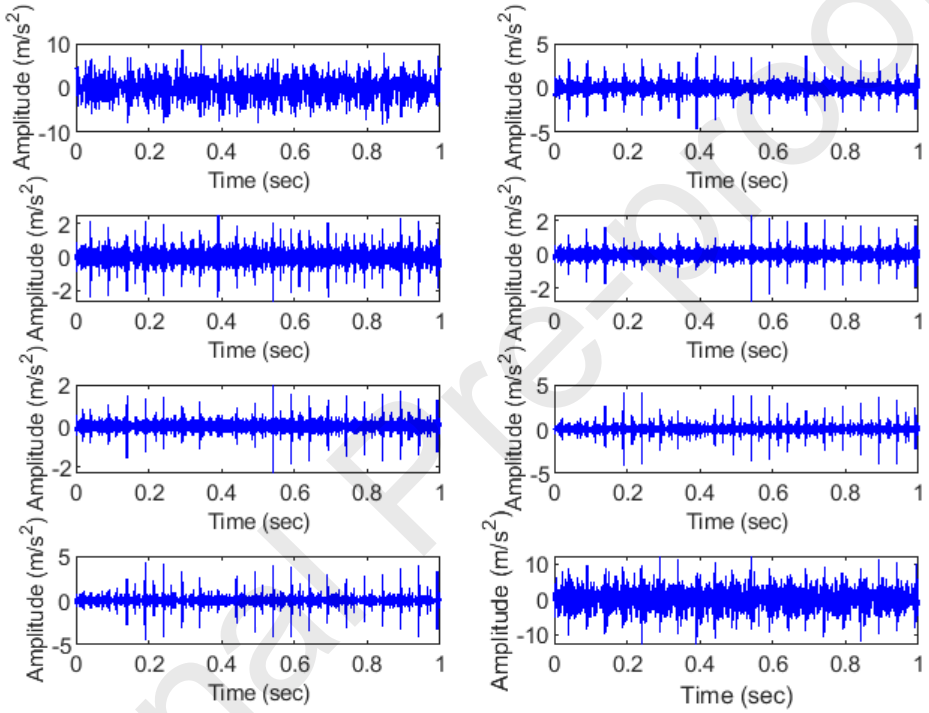

(b)

Fig 4. (a) A typical signal resulted from defect free condition and (b) Decomposition of defect free signal into 8 **WPT3** bands using 3- level MODWPT

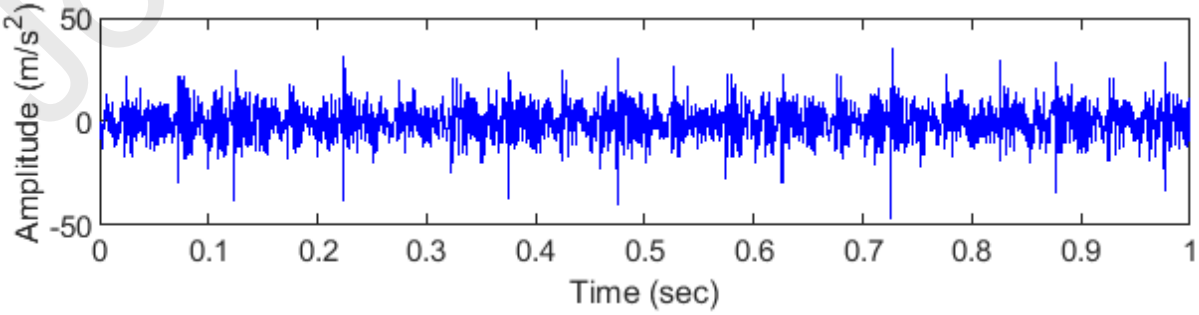

(a)

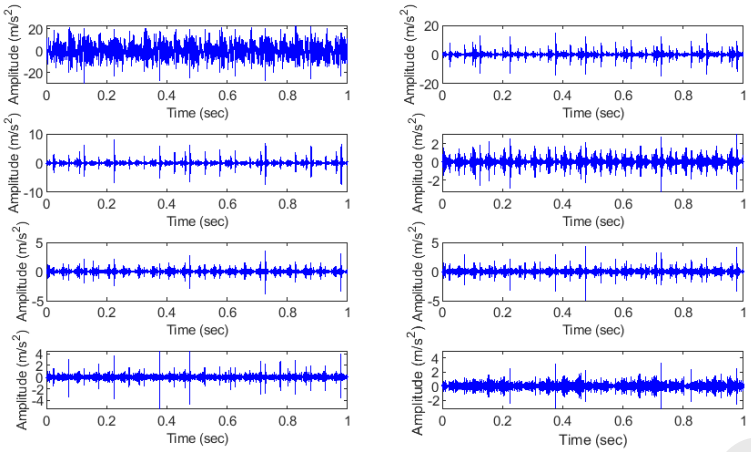

(b)

Fig 5. (a) A typical signal resulted from angular misalignment of 10 Mils and (b) Decomposition of angular misalignment signal into 8 **WPT3** bands using 3- level MODWPT

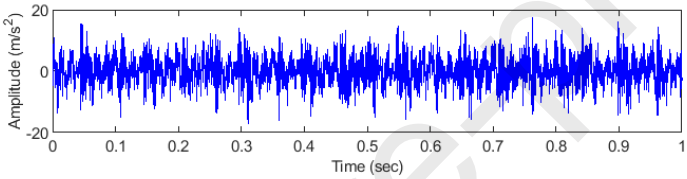

(a)

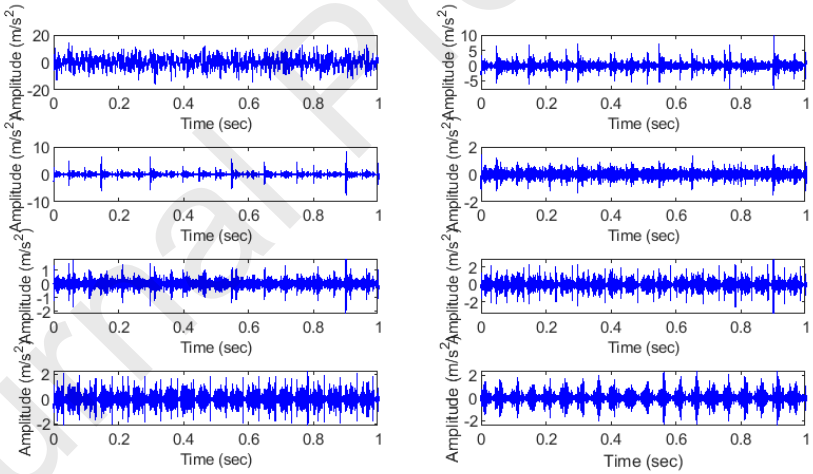

(b)

Fig 6. (a) A typical signal resulted from parallel misalignment of 10 Mils and (b) Decomposition of parallel misalignment signal into 8 **WPT3** bands using 3- level MODWPT

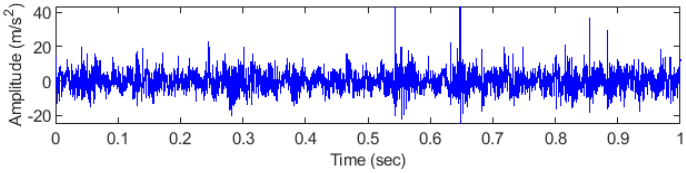

(a)

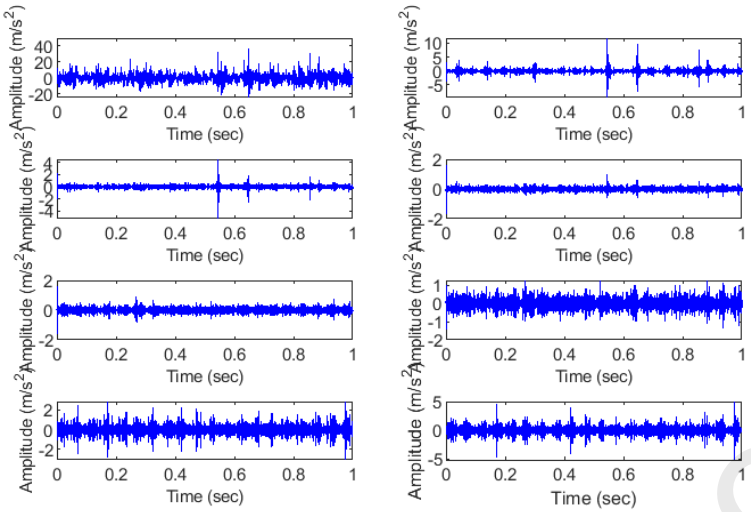

(b)

Fig 7. (a) A typical signal resulted from unbalance condition and (b) Decomposition of unbalance signal into 8 **WPT3** bands using 3- level MODWPT

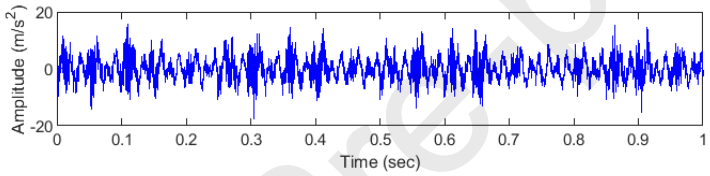

(a)

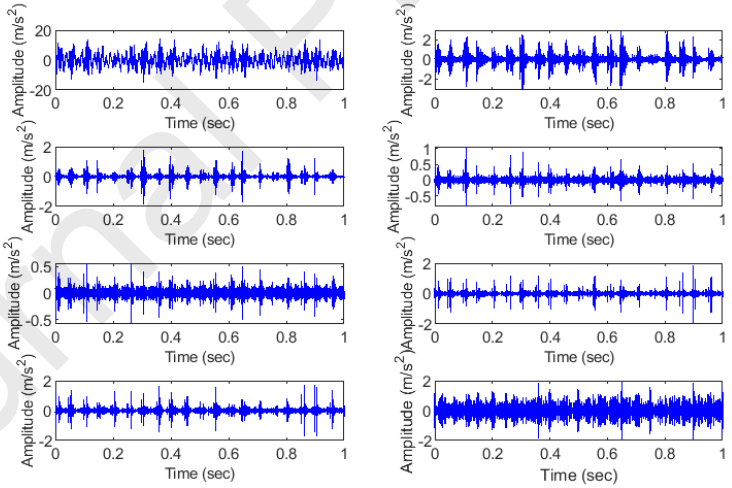

(b)

Fig 8. (a) A typical signal representing rub condition and (b) Decomposition of rub signal into 8 **WPT3** bands using 3- level MODWPT

Step 3: - Normalization of Decomposed Signals

A schematic flow chart representing the proclaimed bipolar neutrosophic cross entropy and 3-level MODWPT based rotor defect identification methodology is displayed in **Fig 1**. In

the underlying study, we have applied 3-level MODWPT for the purpose of generating eight sub-frequency bands called as **WPT3** bands. In our notations, the symbol E is called as energy vector, which can be constructed by utilizing the energy readings of various rotor defect conditions at 8 **WPT3** bands and expressed by **(13).**

$$E = \left[e_3^0, e_3^1, e_3^2, e_3^3, e_3^4, e_3^5, e_3^6, e_3^7\right] \quad .. (13)$$

Because the vibration data may be noisy and hence conflicting for fuzzification, it becomes necessary before fuzzification to transform the energy vector **(13)** to lie in the closed interval $[0,1]$. Let Max.e_3 and Min.e_3 respectively abbreviate as maximum and minimum monitored energy readings at eight **WPT3** bands. Then, the normalized energy vector, represented by E^*, can be constructed as given by **(14).**

$$E^* = \left[e_3^{*0}, e_3^{*1}, e_3^{*2}, e_3^{*3}, e_3^{*4}, e_3^{*5}, e_3^{*6}, e_3^{*7}\right]; e_3^{*k} = \frac{e_3^k - \text{Min}.e_3^k}{\text{Max}.e_3^k - \text{Min}.e_3^k}; k = 0,1,2,...7. \quad \ldots (14)$$

Step:-4 Computation of Lower and Upper Energy Bounds

Corresponding to each familiar and unfamiliar rotor defect conditions under study, the energy vector **(14)** has discriminating distribution at each **WPT3** bands. Let

$\tilde{\mu}_{B_K}(x_i) =$ The truth membership degree (It is the lower energy bound and can be extracted from the normalized energy readings of training samples of K^{th} familiar rotor defect condition at i^{th} **WPT3** band). Let

$\tilde{U}_{B_K}(x_i) =$ The upper energy bound which can be extracted from the normalized energy readings of training samples K^{th} familiar rotor defect condition at i^{th} **WPT3** band. Then, the set:

$\left(< x_1, [\tilde{\mu}_{B_K}(x_1), \tilde{U}_{B_K}(x_1)] >, < x_2, [\tilde{\mu}_{B_K}(x_2), \tilde{U}_{B_K}(x_2)] >, ..., < x_8, [\tilde{\mu}_{B_K}(x_8), \tilde{U}_{B_K}(x_8)] >\right)$

,called as energy intervals, can be constructed for each familiar rotor defect conditions. Let

$\tilde{\mu}_{F_{T_J}}(x_i)$ = The truth membership degree (It is the lower energy bound and can be extracted from the normalized energy readings of testing samples of J^{th} unfamiliar rotor defect condition at i^{th} **WPT3** band). Let

$\tilde{U}_{F_{T_J}}(x_i)$ = The upper energy bound which can be extracted from the normalized energy readings of testing samples J^{th} familiar rotor defect condition at i^{th} **WPT3** band. Then, the set:

$$\left(< x_1, \left[\tilde{\mu}_{F_{T_J}}(x_1), \tilde{U}_{F_{T_J}}(x_1)\right] >, < x_2, \left[\tilde{\mu}_{F_{T_J}}(x_2), \tilde{U}_{F_{T_J}}(x_2)\right] >, ..., < x_8, \left[\tilde{\mu}_{F_{T_J}}(x_8), \tilde{U}_{F_{T_J}}(x_8)\right] >\right),$$

called as energy intervals, can be constructed for each unfamiliar rotor defect conditions.

Step:-5 Construction of Fuzzy, Neutrosophic and Bipolar neutrosophic Sets

The experimentation investigations and data observations carried out in the underlying study has made us capable for extracting the truth membership degrees (lower energy bounds) and

upper energy bounds. Suppose the rotor element in our study experiences some familiar defect conditions at eight **WPT3** band and we represent this knowledge by the set B_K $(K = 1,2,3,4,5)$ as shown in **Table 1.** other words, the various familiar rotor defect conditions in this study are represented by the set $B_K = (B_1,B_2,B_3,B_4,B_5)$ where B_1 = Defect free condition, B_2 = Angular misalignment of 10 Mils, B_3 = Parallel misalignment of 10 Mils, B_4 = Rub and $B_5 =$ Unbalance.

Similarly, we can denote various unfamiliar rotor defect conditions by the set F_{T_j} $(j = 1,2,3,4,5)$ at eight **WPT3** band.

In our notations, $\tilde{\mu}_{B_K}(x_i)$ denotes the truth membership degree of K^{th} familiar rotor defect condition at i^{th} **WPT3** band. Also, $\tilde{U}_{B_K}(x_i)$ denotes the upper energy bound of K^{th} familiar rotor defect condition at i^{th} **WPT3** band. Therefore,

The amount of fuzziness based on indeterminacy membership degree of K^{th} familiar rotor defect condition at i^{th} **WPT3** band can be defined as $\tilde{f}_{B_K}(x_i) = 1 - \tilde{U}_{B_K}(x_i)$ $,i = 1,2,\ldots,8,K = 1,2,3,4,5$. Similarly, the amount of fuzziness based on falsity membership degree of K^{th} familiar rotor defect condition at i^{th} **WPT3** band can be defined as $\tilde{i}_{B_K}(x_i) = 1 - \tilde{f}_{B_K}(x_i) - \tilde{U}_{B_K}(x_i),i = 1,2,\ldots,8,K = 1,2,3,4,5.$

In this study, the value of $\tilde{i}_{B_K}(x_i)$ is restricted to $0 \cdot 001$ if it returns any other value which is less than or equal to $0 \cdot 001$.Next, the set $B_K(K = 1,2,3,4,5)$ of various familiar rotor defect conditions can be extended into the desired forms as follows:

(a) Into the form of fuzzy sets. The desired version of the set B_K into the form of fuzzy sets can be described by **(15).**

$$B_K = (< x_1,\tilde{\mu}_{B_K}(x_1) >, < x_2,\tilde{\mu}_{B_K}(x_2) >,\ldots, < x_8,\tilde{\mu}_{B_K}(x_8) >) \quad \ldots (15)$$

(b) Into the form of single valued neutrosophic sets. The extended version of the set B_K into the form of single valued neutrosophic sets can be described by **(16).**

$$B_K = (< x_1,\tilde{\mu}_{B_K}(x_1),\tilde{i}_{B_K}(x_1),\tilde{f}_{B_K}(x_1) >, < x_2,\tilde{\mu}_{B_K}(x_2),\tilde{i}_{B_K}(x_2),\tilde{f}_{B_K}(x_2) >,\ldots, < x_8,\tilde{\mu}_{B_K}(x_8),\tilde{i}_{B_K}(x_8),\tilde{f}_{B_K}(x_8) >) \quad \ldots (16)$$

(c) Into the form of bipolar neutrosophic sets.

Because the vibration data may be conflicting in certain situations, it becomes necessary to convert the representation **(16)** of each familiar rotor defect condition B_K to the form of bipolar neutrosophic sets. This conversion is, however not burdensome, but shrewd and can be done as described by **(17).**

$$B_K = \begin{pmatrix} < x_1,\tilde{\mu}^+_{B_K}(x_1),\tilde{i}^+_{B_K}(x_1),\tilde{f}^+_{B_K}(x_1),\tilde{\mu}^-_{B_K}(x_1),\tilde{i}^-_{B_K}(x_1),\tilde{f}^-_{B_K}(x_1) >, \\ < x_2,\tilde{\mu}^+_{B_K}(x_2),\tilde{i}^+_{B_K}(x_2),\tilde{f}^+_{B_K}(x_2),\tilde{\mu}^-_{B_K}(x_2),\tilde{i}^-_{B_K}(x_2),\tilde{f}^-_{B_K}(x_2) >, \\ \vdots \\ < x_8,\tilde{\mu}^+_{B_K}(x_8),\tilde{i}^+_{B_K}(x_8),\tilde{f}^+_{B_K}(x_8),\tilde{\mu}^-_{B_K}(x_8),\tilde{i}^-_{B_K}(x_8),\tilde{f}^-_{B_K}(x_8) > \end{pmatrix} \quad \ldots (17)$$

Similarly, the various unfamiliar rotor defect conditions F_{T_j} can also be described by the

form of fuzzy sets (**Eq. 18)**, single valued neutrosophic sets (**Eq. 19)**, as well as bipolar neutrosophic sets (**Eq. 20)**, as follows.

$$F_{T_J} = \left(< x_1,\tilde{\mu}_{F_{T_J}}(x_1) > , < x_2,\tilde{\mu}_{F_{T_J}}(x_2) > ,..., < x_8,\tilde{\mu}_{F_{T_J}}(x_8) > \right) \quad \cdots (18)$$

$$F_{T_J} = \left(< x_1,\tilde{\mu}_{F_{T_J}}(x_1),\tilde{i}_{F_{T_J}}(x_1),\tilde{f}_{F_{T_J}}(x_1) > , < x_2,\tilde{\mu}_{F_{T_J}}(x_2),\tilde{i}_{F_{T_J}}(x_2),\tilde{f}_{F_{T_J}}(x_2) > ,..., < x_8,\tilde{\mu}_{F_{T_J}}(x_8),\tilde{i}_{F_{T_J}}(x_8),\tilde{f}_{F_{T_J}}(x_8) > \right) \quad \cdots (19)$$

$$F_{T_J} = \begin{pmatrix} < x_1,\tilde{\mu}^+_{F_{T_J}}(x_1),\tilde{i}^+_{F_{T_J}}(x_1),\tilde{f}^+_{F_{T_J}}(x_1),\tilde{\mu}^-_{F_{T_J}}(x_1),\tilde{i}^-_{F_{T_J}}(x_1),\tilde{f}^-_{F_{T_J}}(x_1) > , \\ < x_2,\tilde{\mu}^+_{F_{T_J}}(x_2),\tilde{i}^+_{F_{T_J}}(x_2),\tilde{f}^+_{F_{T_J}}(x_2),\tilde{\mu}^-_{F_{T_J}}(x_2),\tilde{i}^-_{F_{T_J}}(x_2),\tilde{f}^-_{F_{T_J}}(x_2) > , \\ . \\ . \\ < x_8,\tilde{\mu}^+_{F_{T_J}}(x_8),\tilde{i}^+_{F_{T_J}}(x_8),\tilde{f}^+_{F_{T_J}}(x_8),\tilde{\mu}^-_{F_{T_J}}(x_8),\tilde{i}^-_{F_{T_J}}(x_8),\tilde{f}^-_{F_{T_J}}(x_8) > \end{pmatrix} \quad \cdots (20)$$

Step: -6 Computation of Cross Entropy Measure Values

(a) If we Set $U_0 = \tilde{\mu}_{B_K}(x_i) + \tilde{\mu}_{F_{T_J}}(x_i), U_1 = \sqrt{\tilde{\mu}_{B_K}(x_i)} + \sqrt{\tilde{\mu}_{F_{T_J}}(x_i)}, U_2 = \sqrt{1 - \tilde{\mu}_{B_K}(x_i)} + \sqrt{1 - \tilde{\mu}_{F_{T_J}}(x_i)}$, then

In this study, the number of familiar defect conditions is described by K=1,2,3,4,5 and the number of unfamiliar defect conditions is described by J=1,2,3,4,5. Also, the number of **WPT3** bands in this study is described by $i = 1,2,...,8$.. Let the symmetric fuzzy cross entropy measure values between each familiar (B_K) and unfamiliar (F_{T_J}) rotor defects conditions are represented by $H^{\mu}_{CE}(B_K,F_{T_J})$. Then, it can be evaluated by considering $i = 1,2,...,8$, and replacing $\tilde{A}_{FS} = \left(< x_i,\tilde{\mu}_{A^f}(x_i) > \right)$; $\tilde{B}_{FS} = \left(< x_i,\tilde{\mu}_{B^f}(x_i) > \right)$ with $B_K = \left(< x_i,\tilde{\mu}_{B_K}(x_i) > \right)$;$F_{T_J} = \left(< x_i,\tilde{\mu}_{F_{T_J}}(x_i) > \right)$ into the resulting equation **(1)** which yields **(21).**

$$H^{\mu}_{CE}(B_K,F_{T_J}) = \sum_{i=1}^{8}\left[-8tanh^{-1}\frac{1}{2} + (3+U_0)tanh^{-1}\left(\frac{1+U_0^2+U_1^2}{2+(2+U_0)U_1^2}\right) + (5-U_0)tanh^{-1}\left(\frac{1+(2-U_0)^2+U_2^2}{2+(4-U_0)U_2^2}\right)\right] \quad \ldots (21)$$

(b) Let the symmetric single valued neutrosophic cross entropy measure values between various familiar (B_K) and unfamiliar (F_{T_J}) rotor defect conditions are denoted by $S_{CE}(B_K,F_{T_J})$. Then, it can be evaluated by considering $i = 1,2,...,8$, and replacing $\tilde{A}^n_{SV} = \left(< x_i,\tilde{\mu}_{A^f}(x_i),\tilde{i}_{A^f}(x_i),\tilde{f}_{A^f}(x_i) > \right)$;$\tilde{B}^n_{SV} = \left(< x_i,\tilde{\mu}_{B^f}(x_i),\tilde{i}_{B^f}(x_i),\tilde{f}_{B^f}(x_i) > \right)$ with $B_K = \left(< x_i,\tilde{\mu}_{B_K}(x_i),\tilde{i}_{B_K}(x_i),\tilde{f}_{B_K}(x_i) > \right)$;$F_{T_J} = \left(< x_i,\tilde{\mu}_{F_{T_J}}(x_i),\tilde{i}_{F_{T_J}}(x_i),\tilde{f}_{F_{T_J}}(x_i) > \right)$ into **(10)** to get **(22).**

$$S_{CE}(B_K,F_{T_J}) =$$

$$\sum_{i=1}^{8}\left[-8tanh^{-1}\frac{1}{2}+(3+U_0)tanh^{-1}\left(\frac{1+U_0^2+U_1^2}{2+(2+U_0)U_1^2}\right)+(5-U_0)tanh^{-1}\left(\frac{1+(2-U_0)^2+U_2^2}{2+(4-U_0)U_2^2}\right)\right]$$
$$+\sum_{i=1}^{8}\left[-8tanh^{-1}\frac{1}{2}+(3+I_0)tanh^{-1}\left(\frac{1+I_0^2+I_1^2}{2+(2+I_0)I_1^2}\right)+(5-I_0)tanh^{-1}\left(\frac{1+(2-I_0)^2+I_2^2}{2+(4-I_0)I_2^2}\right)\right]$$
$$+\sum_{i=1}^{8}\left[-8tanh^{-1}\frac{1}{2}+(3+F_0)tanh^{-1}\left(\frac{1+F_0^2+F_1^2}{2+(2+F_0)F_1^2}\right)+(5-F_0)tanh^{-1}\left(\frac{1+(2-F_0)^2+F_2^2}{2+(4-F_0)F_2^2}\right)\right]$$

.. (22)

(c) Let the symmetric bipolar neutrosophic cross entropy measure values between various familiar (B_K) and unfamiliar (F_{T_j}) rotor defect conditions are represented by $T_{CE}(B_K,F_{T_j})$. Then, it can be evaluated by considering $i = 1,2,...,8$, and replacing

$\tilde{\mu}_{A^f}^{+}(x_i),\tilde{i}_{A^f}^{+}(x_i),\tilde{f}_{A^f}^{+}(x_i)$ with $\mu_{B_K}^{+}(x_i),i_{B_K}^{+}(x_i),f_{B_K}^{+}(x_i)$;

$\tilde{\mu}_{A^f}^{-}(x_i),\tilde{i}_{A^f}^{-}(x_i),\tilde{f}_{A^f}^{-}(x_i)$ with $\mu_{B_K}^{-}(x_i),i_{B_K}^{-}(x_i),f_{B_K}^{-}(x_i)$;

$\tilde{\mu}_{B^f}^{+}(x_i),\tilde{i}_{B^f}^{+}(x_i),\tilde{f}_{B^f}^{+}(x_i)$ with $\tilde{\mu}_{F_{T_j}}^{+}(x_i),\tilde{i}_{F_{T_j}}^{+}(x_i),\tilde{f}_{F_{T_j}}^{+}(x_i)$; and

$\tilde{\mu}_{B^f}^{-}(x_i),\tilde{i}_{B^f}^{-}(x_i),\tilde{f}_{B^f}^{-}(x_i)$ with $\tilde{\mu}_{F_{T_j}}^{-}(x_i),\tilde{i}_{F_{T_j}}^{-}(x_i),\tilde{f}_{F_{T_j}}^{-}(x_i)$ into (**11**) to get (**23**). Thus,

$T_{CE}(B_K,F_{T_j}) =$

$$\sum_{i=1}^{n}\left[\begin{array}{r}-16tanh^{-1}\frac{1}{2}+(3+U_0^{+})tanh^{-1}\left(\frac{1+U_0^{+2}+U_1^{+2}}{2+(2+U_0^{+})U_1^{+2}}\right)+(5-U_0^{+})tanh^{-1}\left(\frac{1+(2-U_0^{+})^2+U_2^{+2}}{2+(4-U_0^{+})U_2^{+2}}\right)\\ +(3-U_0^{-})tanh^{-1}\left(\frac{1+U_0^{-2}+U_1^{-2}}{2+(2-U_0^{-})U_1^{-2}}\right)+(5+U_0^{-})tanh^{-1}\left(\frac{1+(2+U_0^{-})^2+U_2^{-2}}{2+(4+U_0^{-})U_2^{-2}}\right)\end{array}\right]$$

$+$

$$\sum_{i=1}^{n}\left[\begin{array}{r}-16tanh^{-1}\frac{1}{2}+(3+I_0^{+})tanh^{-1}\left(\frac{1+I_0^{+2}+I_1^{+2}}{2+(2+I_0^{+})I_1^{+2}}\right)+(5-I_0^{+})tanh^{-1}\left(\frac{1+(2-I_0^{+})^2+I_2^{+2}}{2+(4-I_0^{+})I_2^{+2}}\right)\\ +(3-I_0^{-})tanh^{-1}\left(\frac{1+I_0^{-2}+I_1^{-2}}{2+(2-I_0^{-})I_1^{-2}}\right)+(5+I_0^{-})tanh^{-1}\left(\frac{1+(2+I_0^{-})^2+I_2^{-2}}{2+(4+I_0^{-})I_2^{-2}}\right)\end{array}\right]$$

$+$

$$\sum_{i=1}^{n}\left[\begin{array}{r}-16tanh^{-1}\frac{1}{2}+(3+F_0^{+})tanh^{-1}\left(\frac{1+F_0^{+2}+F_1^{+2}}{2+(2+F_0^{+})F_1^{+2}}\right)+(5-F_0^{+})tanh^{-1}\left(\frac{1+(2-F_0^{+})^2+F_2^{+2}}{2+(4-F_0^{+})F_2^{+2}}\right)\\ +(3-F_0^{-})tanh^{-1}\left(\frac{1+F_0^{-2}+F_1^{-2}}{2+(2-F_0^{-})F_1^{-2}}\right)+(5+F_0^{-})tanh^{-1}\left(\frac{1+(2+F_0^{-})^2+F_2^{-2}}{2+(4+F_0^{-})F_2^{-2}}\right)\end{array}\right]$$

… (23)

Here, the notations with their expressions have been provided in APPENDIX-A.2.

Step: -7 Identification of Rotor Defects Using Minimum Cross Entropy Measure Values

The minimum symmetric cross entropy measure values of $H^{\mu}_{CE}(B_K,F_{T_j})$,$S_{CE}(B_K,F_{T_j})$or $T_{CE}(B_K,F_{T_j})$ indicate that B_K is closer F_{T_j}. In other words, the optimal rotor fault type selection can be justified according to the minimum cross entropy values returned by equations (**21-23).**

The overhead discussion has put us in a conclusive situation to demonstrate the applicability and effectiveness of the proposed symmetric bipolar neutrosophic cross entropy and MODWPT based methodology as follows.

7. IDENTIFICATION OF ROTOR DEFECTS

The block diagram represented by **Fig. 1** depicts the proposed rotor defect identification methodology. The various familiar rotor defect conditions in this study are represented by the set $B_K=(B_1,B_2,B_3,B_4,B_5)$ where B_1 = Defect free condition, B_2 = Angular misalignment of 10 Mils, B_3 = Parallel misalignment of 10 Mils, B_4 = Rub and $B_5=$ Unbalance.

Step:-1-3 A lot of experimentation investigations and data observations carried out in the underlying study has made us capable for extracting the truth membership degrees (lower energy bounds) and upper energy bounds for various familiar and unfamiliar rotor defect conditions at each eight **WPT3** bands.

Table 2. Energy intervals of familiar rotor defect conditions $B_K(K=1,2,3,4,5)$ at eight **WPT3** bands

	WPT3-1	**WPT3- 2**	**WPT3- 3**	**WPT3- 4**	**WPT3- 5**	**WPT3- 6**	**WPT3- 7**	**WPT3- 8**
B_1: Defect Free	[0·00,0·01]	[0·01,0·01]	[0·01,0·01]	[0·01,0·01]	[0·01,0·01]	[0·01,0·02]	[0·01,0·01]	[0·01,0·01]
B_2: Angular Misalignment	[0·26,0·28]	[0·03,0·04]	[0·01,0·01]	[0·02,0·03]	[0·02,0·02]	[0·01,0·02]	[0·01,0·01]	[0·01,0·02]
B_3: Parallel Misalignment	[0·07,0·08]	[0·02,0·02]	[0·01,0·01]	[0·01,0·01]	[0·01,0·02]	[0·01,0·02]	[0·01,0·01]	[0·01,0·02]
B_4: Rub	[0·05,0·06]	[0·01,0·01]	[0·00,0·01]	[0·00,0·01]	[0·00,0·01]	[0·00,0·01]	[0·00,0·01]	[0·02,0·03]
B_5: Unbalance	[0·74,0·90]	[0·69,0·98]	[0·70,0·97]	[0·66,0·88]	[0·58,0·88]	[0·60,0·85]	[0·44,0·76]	[0·55,0·83]

Table 3. Energy interval ranges of unfamiliar rotor defect conditions $F_{T_j}(j=1,2,3,4,5)$ at eight **WPT3** bands

	WPT3-1	**WPT3- 2**	**WPT3- 3**	**WPT3- 4**	**WPT3- 5**	**WPT3- 6**	**WPT3- 7**	**WPT3- 8**
F_{T_1} : Defect Free	[0·00,0·01]	[0·01,0·01]	[0·01,0·01]	[0·01,0·02]	[0·01,0·01]	[0·01,0·02]	[0·01,0·01]	[0·01,0·01]
F_{T_2} : Angular Misalignment	[0·19,0·29]	[0·02,0·04]	[0·01,0·02]	[0·02,0·04]	[0·02,0·03]	[0·01,0·03]	[0·01,0·01]	[0·01,0·02]
F_{T_3} : Parallel Misalignment	[0·06,0·08]	[0·02,0·02]	[0·01,0·01]	[0·01,0·01]	[0·01,0·02]	[0·01,0·02]	[0·01,0·01]	[0·01,0·02]
F_{T_4} : Rub	[0·05,0·06]	[0·01,0·01]	[0·01,0·01]	[0·01,0·01]	[0·01,0·01]	[0·01,0·01]	[0·01,0·01]	[0·02,0·05]
F_{T_5} : Unbalance	[0·70,1·00]	[0·67,1·00]	[0·69,1·00]	[0·58,1·00]	[0·53,1·00]	[0·57,1·00]	[0·52,1·00]	[0·50,1·00]

Table 4. Representing energy interval of B_K into the form of fuzzy sets and single valued neutrosophic sets at eight **WPT3** bands

WPT-1	**WPT- 2**	**WPT- 3**	**WPT- 4**	**WPT- 5**	**WPT- 6**	**WPT- 7**	**WPT- 8**
B_1 :[0·00,0·01,0.99]	[0·01,0·00,0.99]	[0·01,0·00,0.99]	[0·01,0·00,0.99]	[0·01,0·00,0.99]	[0·01,0·01,0.98]	[0·01,0·00,0.99]	[0·01,0·00,0.99]
B_2 :[0·26,0·02,0.72]	[0·03,0·01,0.96]	[0·01,0·00,0.99]	[0·02,0·01,0.97]	[0·02,0·00,0.98]	[0·01,0·01,0.98]	[0·01,0·00,0.99]	[0·01,0·01,0.98]
B_3 :[0·07,0·01,0.92]	[0·02,0·00,0.98]	[0·01,0·00,0.99]	[0·01,0·00,0.99]	[0·01,0·01,0.98]	[0·01,0·01,0.98]	[0·01,0·00,0.99]	[0·01,0·01,0.98]
B_4 :[0·05,0·01,0.94]	[0·01,0·00,0.99]	[0·00,0·01,0.99]	[0·00,0·01,0.99]	[0·00,0·01,0.99]	[0·00,0·01,0.99]	[0·00,0·01,0.99]	[0·02,0·01,0.97]
B_5 :[0·74,0·16,0.10]	[0·69,0·29,0.02]	[0·70,0·27,0.03]	[0·66,0·22,0.12]	[0·58,0·30,0.12]	[0·60,0·25,0.15]	[0·44,0·32,0.24]	[0·55,0·28,0.17]

.

Step:-4 The energy intervals $\left[\tilde{\mu}_{B_K}(x_i),\tilde{U}_{B_K}(x_i)\right];i=1,2,...,8,K=1,2,...,5$ of each familiar rotor defect condition B_K at each eight **WPT3** bands can be constructed employing the proposed methodology (**Fig.1)** and represented in **Table 2.**

Similarly, the energy intervals $\left[\tilde{\mu}_{F_{T_j}}(x_i),\tilde{U}_{F_{T_j}}(x_i)\right];i=1,2,..,8,K=1,2,...,5$ of each unfamiliar rotor defect conditions F_{T_j} at each eight **WPT3** bands can also be constructed employing the proposed methodology (**Fig.1)** and represented in **Table 3.**

Table 5. Representing energy interval ranges of F_{T_j} into the form of fuzzy sets and single valued neutrosophic sets at eight **WPT3** bands

WPT3-1	**WPT3- 2**	**WPT3- 3**	**WPT3- 4**	**WPT3- 5**	**WPT3- 6**	**WPT3- 7**	**WPT3- 8**
F_{T_1} :[0·00,0·01,0.99]	[0·01,0·00,0.99]	[0·01,0·00,0.99]	[0·01,0·01,0.98]	[0·01,0·00,0.99]	[0·01,0·01,0.98]	[0·01,0·00,0.99]	[0·00,0·01,0.99]
F_{T_2} :[0·19,0·10,0.71]	[0·02,0·02,0.96]	[0·01,0·01,0.98]	[0·02,0·02,0.96]	[0·02,0·01,0.97]	[0·01,0·02,0.97]	[0·01,0·00,0.99]	[0·01,0·01,0.98]
F_{T_3} :[0·06,0·02,0.92]	[0·02,0·00,0.98]	[0·01,0·00,0.99]	[0·01,0·00,0.99]	[0·01,0·01,0.98]	[0·01,0·01,0.98]	[0·01,0·00,0.99]	[0·01,0·01,0.98]
F_{T_4} :[0·05,0·01,0.94]	[0·00,0·01,0.99]	[0·01,0·00,0.99]	[0·01,0·00,0.99]	[0·01,0·00,0.99]	[0·01,0·00,0.99]	[0·01,0·00,0.99]	[0·02,0·03,0.95]
F_{T_5} :[0·70,0·30,0.00]	[0·67,0·33,0.00]	[0·69,0·31,0.00]	[0·58,0·42,0.00]	[0·53,0·47,0.00]	[0·57,0·43,0.00]	[0·52,0·48,0.00]	[0·50,0·50,0.00]

Step: -5 The energy intervals of each B_K and F_{T_j} are further extended into the form of fuzzy sets and single valued neutrosophic sets as shown in **Table 4** and **Table 5.**

Step: -6 The single valued neutrosophic sets of each B_K and F_{T_j} are finally converted into the form of bipolar neutrosophic sets and represented in **Table 6** and **Table 7.**

Step:-7 The symmetric fuzzy cross entropy values $H^{\mu}_{CE}(B_K,F_{T_j})$ (**Method 1**),single

Table 6. Representing single valued neutrosophic sets of each B_K into the form of bipolar neutrosophic sets (BNSs) at eight **WPT3** bands

B_1: $[0\cdot00,0\cdot01,0.99,-0.01,-0.02,-1.00]$	$[0\cdot01,0\cdot00,0.99,-0.02,-0.01,-1.00]$	$[0\cdot01,0\cdot00,0.99,-0.02,-0.01,-1.00]$
$[0\cdot01,0\cdot00,0.99,-0.02,-0.01,-1.00]$	$[0\cdot01,0\cdot00,0.99,-0.02,-0.01,-1.00]$	$[0\cdot01,0\cdot01,0.98,-0.02,-0.02,-0.99]$
$[0\cdot01,0\cdot00,0.99,-0.02,-0.01,-1.00]$	$[0\cdot01,0\cdot00,0.99,-0.02,-0.01,-1.00]$	
B_2: $[0\cdot26,0\cdot02,0.72,-0.27,-0.03,-0.73]$	$[0\cdot03,0\cdot01,0.96,-0.04,-0.02,-0.97]$	$[0\cdot01,0\cdot00,0.99,-0.02,-0.01,-1.00]$
$[0\cdot02,0\cdot01,0.97,-0.03,-0.02,-0.98]$	$[0\cdot02,0\cdot00,0.98,-0.03,-0.01,-0.99]$	$[0\cdot01,0\cdot01,0.98,-0.02,-0.02,-0.99]$
$[0\cdot01,0\cdot00,0.99,-0.02,-0.01,-1.00]$	$[0\cdot01,0\cdot01,0.98,-0.02,-0.02,-0.99]$	
B_3: $[0\cdot07,0\cdot01,0.92,-0.08,-0.02,-0.93]$	$[0\cdot02,0\cdot00,0.98,-0.03,-0.01,-0.99]$	$[0\cdot01,0\cdot00,0.99,-0.02,-0.01,-1.00]$
$[0\cdot01,0\cdot00,0.99,-0.02,-0.01,-1.00]$	$[0\cdot01,0\cdot01,0.98,-0.02,-0.02,-0.99]$	$[0\cdot01,0\cdot01,0.98,-0.02,-0.02,-0.99]$
$[0\cdot01,0\cdot00,0.99,-0.02,-0.01,-1.00]$	$[0\cdot01,0\cdot01,0.98,-0.02,-0.02,-0.99]$	
B_4: $[0\cdot05,0\cdot01,0.94,-0.06,-0.02,-0.95]$	$[0\cdot01,0\cdot00,0.99,-0.02,-0.01,-1.00]$	$[0\cdot00,0\cdot01,0.99,-0.01,-0.02,-1.00]$
$[0\cdot00,0\cdot01,0.99,-0.01,-0.02,-1.00]$	$[0\cdot00,0\cdot01,0.99,-0.01,-0.02,-1.00]$	$[0\cdot00,0\cdot01,0.99,-0.01,-0.02,-1.00]$
$[0\cdot00,0\cdot01,0.99,-0.01,-0.02,-1.00]$	$[0\cdot02,0\cdot01,0.97,-0.03,-0.02,-0.98]$	
B_5: $[0\cdot74,0\cdot16,0.10,-0.75,-0.17,-0.11]$	$[0\cdot69,0\cdot29,0.02,-0.70,-0.30,-0.03]$	$[0\cdot70,0\cdot27,0.03,-0.71,-0.28,-0.04]$
$[0\cdot66,0\cdot22,0.12,-0.67,-0.23,-0.13]$	$[0\cdot58,0\cdot30,0.12,-0.59,-0.31,-0.13]$	$[0\cdot60,0\cdot25,0.15,-0.61,-0.26,-0.16]$
$[0\cdot44,0\cdot32,0.24,-0.45,-0.33,-0.25]$	$[0\cdot55,0\cdot28,0.17,-0.56,-0.29,-0.18]$	

Table 7. Representing single valued neutrosophic sets of each F_{T_J} into the form of bipolar neutrosophic sets at eight **WPT3** bands

F_{T_1}: $[0.01,0.00,0.99,-0.02,-0.01,-1.00]$	$[0.01,0.00,0.99,-0.02,-0.01,-1.00]$	$[0.01,0.00,0.99,-0.02,-0.01,-1.00]$
$[0.01,0.01,0.98,-0.02,-0.02,-0.99]$	$[0.01,0.00,0.99,-0.02,-0.01,-1.00]$	$[0.01,0.01,0.98,-0.02,-0.02,-0.99]$
$[0.01,0.00,0.99,-0.02,-0.01,-1.00]$	$[0.00,0.01,0.99,-0.01,-0.02,-1.00]$	
F_{T_2}: $[0.19,0.10,0.71,-0.20,-0.11,-0.72]$	$[0.02,0.02,0.96,-0.03,-0.03,-0.97]$	$[0.01,0.01,0.98,-0.02,-0.02,-0.99]$
$[0.02,0.02,0.96,-0.03,-0.03,-0.97]$	$[0.02,0.01,0.97,-0.03,-0.02,-0.98]$	$[0.01,0.02,0.97,-0.02,-0.03,-0.98]$
$[0.01,0.00,0.99,-0.02,-0.01,-1.00]$	$[0.01,0.01,0.98,-0.02,-0.02,-0.99]$	
F_{T_3}: $[0.06,0.02,0.92,-0.07,-0.03,-0.93]$	$[0.02,0.00,0.98,-0.03,-0.01,-0.99]$	$[0.01,0.00,0.99,-0.02,-0.01,-1.00]$
$[0.01,0.00,0.99,-0.02,-0.01,-1.00]$	$[0.01,0.01,0.98,-0.02,-0.02,-0.99]$	$[0.01,0.01,0.98,-0.02,-0.02,-0.99]$
$[0.01,0.00,0.99,-0.02,-0.01,-1.00]$	$[0.01,0.01,0.98,-0.02,-0.02,-0.99]$	
F_{T_4}: $[0.05,0.01,0.94,-0.06,-0.02,-0.95]$	$[0.00,0.01,0.99,-0.01,-0.02,-1.00]$	$[0.01,0.00,0.99,-0.02,-0.01,-1.00]$
$[0.01,0.00,0.99,-0.02,-0.01,-1.00]$	$[0.01,0.00,0.99,-0.02,-0.01,-1.00]$	$[0.01,0.00,0.99,-0.02,-0.01,-1.00]$
$[0.01,0.00,0.99,-0.02,-0.01,-1.00]$	$[0.02,0.03,0.95,-0.03,-0.04,-0.96]$	
F_{T_5}: $[0.70,0.30,0.00,-0.71,-0.31,-0.01]$	$[0.67,0.33,0.00,-0.68,-0.34,-0.01]$	$[0.69,0.31,0.00,-0.70,-0.32,-0.01]$
$[0.58,0.42,0.00,-0.59,-0.43,-0.01]$	$[0.53,0.47,0.00,-0.54,-0.48,-0.01]$	$[0.57,0.43,0.00,-0.58,-0.44,-0.01]$
$[0.52,0.48,0.00,-0.53,-0.49,-0.01]$	$[0.50,0.50,0.00,-0.51,-0.51,-0.01]$	

valued neutrosophic cross entropy values $S_{CE}(B_K,F_{T_j})$ (**Method 2**) and bipolar neutrosophic cross entropy values $T_{CE}(B_K,F_{T_j})$ (**Method 3**) between each B_K and $F_{T_j}$are computed employing equations **(21-23)** and represented in **Table 8(a, b, c).** Using Minimum argument principle, the fault diagnosis order, identified fault conditions and actual fault conditions returned by the proposed methodology (**Methods- 1,2,3)** as well as by the existing cosine similarity measure are represented in **Tables 8(a, b, c, d)**.

The computation time of the proposed algorithm is 1.2 sec.

First Diagnosis Result: - The results of **Tables 8(a, b, c, d)** reveal that, for the first real

testing sample F_{T_1}, the various minimum symmetric cross entropy values are

$H^{\mu}_{CE}(B_K,F_{T_1}) = 0.0002, S_{CE}(B_K,F_{T_1}) = 0.0006, T_{CE}(B_K,F_{T_1}) = 0.0010, C_B(B_K,F_{T_1}) = 0.1124$

Clearly, these values correspond to the defect free condition F_{T_1}. Furthermore, the fact that the minimum cross entropy values correspond to the defect free condition can also be experienced from the three-dimensional bar diagrams shown in **Figs.8(a, b, c, d).**

Second Diagnosis Result:- For the second real testing sample F_{T_2}, , the results provided in **Tables 8(a, b, c, d)** reveal that, the various minimum cross entropy values are

$H^{\mu}_{CE}(B_K,F_{T_2}) = 0.0020, S_{CE}(B_K,F_{T_2}) = 0.0070, T_{CE}(B_K,F_{T_2}) = 0.0142, C_B(B_K,F_{T_2}) = 0.0855$

Clearly, these values correspond to the defect condition F_{T_2} indicating that rotor defect is first resulted from the angular misalignment of 10 Mils. Also, the fact that the various minimum cross entropy values correspond to the defect condition F_{T_2} of angular misalignment of 10 Mils can also be experienced from the three-dimensional bar diagrams as shown in **Figs.8(a, b, c, d).**

Table 8(a) Identification of rotor defects by the minimum cosine similarity measure [1] value based upon bipolar neutrosophic sets

Cosine Similarity Measure	Cosine Similarity Measure values	Fault Diagnosis Order	Fault Condition Identified	Actual Fault Condition
$C_B(B_K,F_{T_1})$	**0**.1124 0.2101 0.1220 0.2548 4.3412	$B_1 \succ B_3 \succ B_2 \succ B_4 \succ B_5$	Defect Free	Defect Free
$C_B(B_K,F_{T_2})$	0.3385 0.0855 0.1671 0.2836 3.5763	$B_2 \succ B_3 \succ B_4 \succ B_1 \succ B_5$	Angular	Angular
$C_B(B_K,F_{T_3})$	0.1189 0.1200 0.0029 0.1880 4.0653	$B_3 \succ B_1 \succ B_2 \succ B_4 \succ B_5$	Parallel	Parallel
$C_B(B_K,F_{T_4})$	0.1752 0.1616 0.1131 0.2771 4.1820	$B_3 \succ B_2 \succ B_1 \succ B_4 \succ B_5$	Parallel	Rub
$C_B(B_K,F_{T_5})$	6.4637 5.8162 6.1255 6.2852 0.8903	$B_5 \succ B_2 \succ B_3 \succ B_4 \succ B_1$	Unbalance	Unbalance

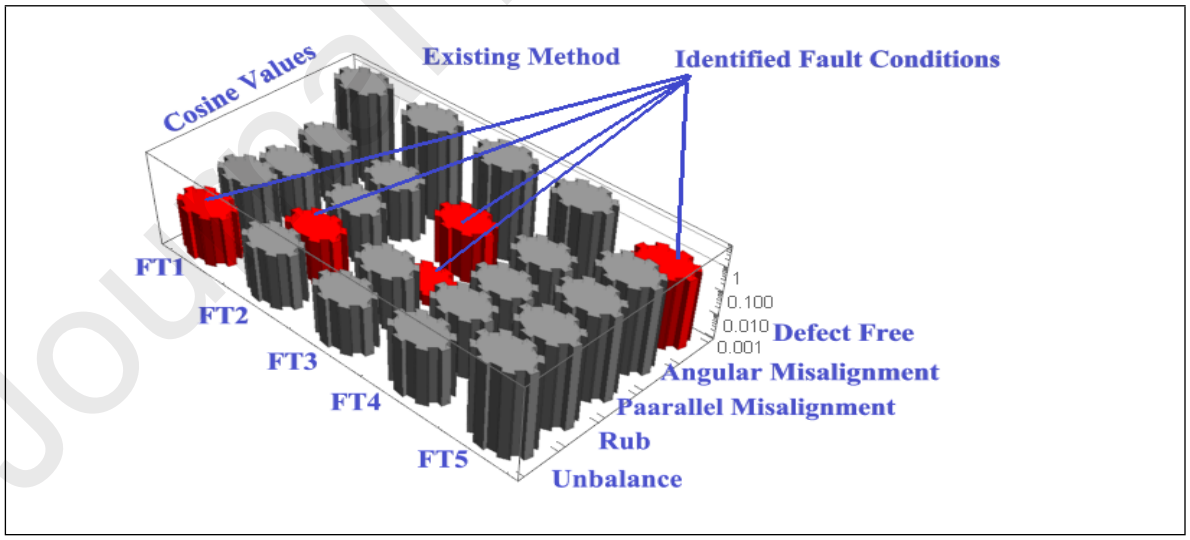

Fig. 8(a) Graphical identification of rotor defects by the existing measure [1] based upon bipolar neutrosophic sets (BNSs)

Third Diagnosis Result: - For the third real testing sample F_{T_3}, the results provided in

Tables 8(a, b, c, d) reveal that, the various minimum symmetric cross entropy values are

$$H^{\mu}_{CE}(B_K,F_{T_3}) = 0.0001, S_{CE}(B_K,F_{T_3}) = 0.0001, T_{CE}(B_K,F_{T_3}) = 0.0002, C_B(B_K,F_{T_3}) = 0.0029$$

These values clearly correspond to the defect condition F_{T_3} which indicates that rotor defect is first resulted from the parallel misalignment of 10 Mils. Also, the fact that the minimum cross entropy values corresponding to the defect condition of parallel misalignment of 10 Mils can also be experienced from the three -dimensional bar diagrams as shown in **Figs.8(a, b, c, d).**

Table 8(b). Identification of rotor defects by the minimum cross entropy measure (**Method-1**) value based on fuzzy sets

Entropy Measure	Fuzzy Cross Entropy Measure Value	Fault Diagnosis Order	Fault Condition Identified	Actual Fault Condition
$H^{\mu}_{CE}(B_K,F_{T_1})$	0.0002 0.0421 0.0025 0.0020 1.9986	$B_1 \succ B_4 \succ B_3 \succ B_2 \succ B_5$	Defect Free	Defect Free
$H^{\mu}_{CE}(B_K,F_{T_2})$	0.0358 0.0020 0.0070 0.0112 1.6187	$B_2 \succ B_3 \succ B_4 \succ B_1 \succ B_5$	Angular	Angular
$H^{\mu}_{CE}(B_K,F_{T_3})$	0.0039 0.0195 0.0001 0.0007 1.7803	$B_3 \succ B_4 \succ B_1 \succ B_2 \succ B_5$	Parallel	Parallel
$H^{\mu}_{CE}(B_K,F_{T_4})$	0.0028 0.0232 0.0007 0.0006 1.9045	$B_4 \succ B_3 \succ B_1 \succ B_2 \succ B_5$	Rub	Rub
$H^{\mu}_{CE}(B_K,F_{T_5})$	1.8664 1.4331 1.6166 2.0406 0.0071	$B_5 \succ B_2 \succ B_3 \succ B_1 \succ B_4$	Unbalance	Unbalance

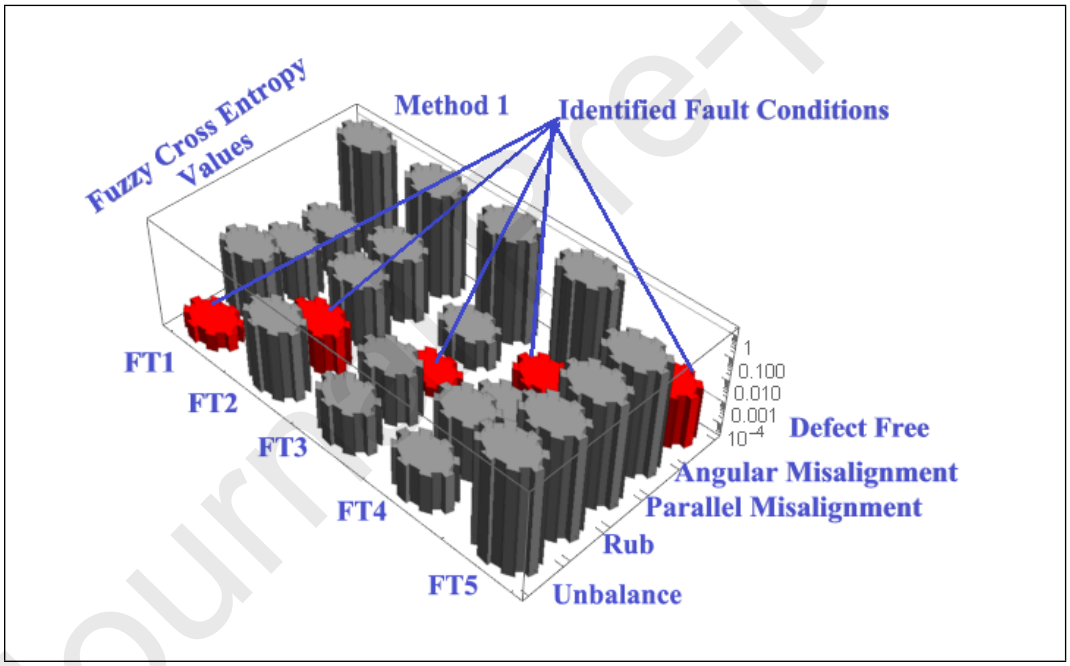

Fig. 8(b). Graphical identification of rotor defects by the proposed cross entropy measure (**Method 1**) based on fuzzy sets

Fourth Diagnosis Result:- For the real testing sample F_{T_4}, the various minimum symmetric cross entropy values are:

$$H^{\mu}_{CE}(B_K,F_{T_4}) = 0.0006, S_{CE}(B_K,F_{T_4}) = 0.0018, T_{CE}(B_K,F_{T_4}) = 0.0029, C_B(B_K,F_{T_4}) = 0.1131$$

Table 8(c) Identification of rotor defects by the minimum cross entropy measure

((**Method-2**) value based on single valued neutrosophic sets (SVNSs)

Entropy Measure	Single Valued Neutrosophic Cross Entropy Measure Values	Fault Diagnosis Order	Fault Condition Identified	Actual Fault Condition
$S_{CE}(B_K,F_{T_1})$	0.0006 0.0918 0.0062 0.0043 6.6173	$B_1 \succ B_4 \succ B_3 \succ B_2 \succ B_5$	Defect Free	Defect Free
$S_{CE}(B_K,F_{T_2})$	0.0933 0.0070 0.0329 0.0424 6.0016	$B_2 \succ B_3 \succ B_4 \succ B_1 \succ B_5$	Angular	Angular
$S_{CE}(B_K,F_{T_3})$	0.0075 0.0386 0.0001 0.0015 6.0850	$B_3 \succ B_4 \succ B_1 \succ B_2 \succ B_5$	Parallel	Parallel
$S_{CE}(B_K,F_{T_4})$	0.0066 0.0486 0.0022 0.0018 6.3316	$B_4 \succ B_3 \succ B_1 \succ B_2 \succ B_5$	Rub	Rub
$S_{CE}(B_K,F_{T_5})$	10.7325 9.2218 9.9266 10.4037 0.2264	$B_5 \succ B_2 \succ B_3 \succ B_1 \succ B_4$	Unbalance	Unbalance

In this case, the minimum cross entropy values correspond to the condition type F_{T_4} which is rub defect condition. Unfortunately, the existing cosine similarity measure fails to identify the desired defect, as can be seen from **Figs. 8(a, b, c, d).** This justifies the superiority of our proposed variants of cross entropy measure based on fuzzy sets, single valued neutrosophic sets and bipolar neutrosophic sets consecutively.

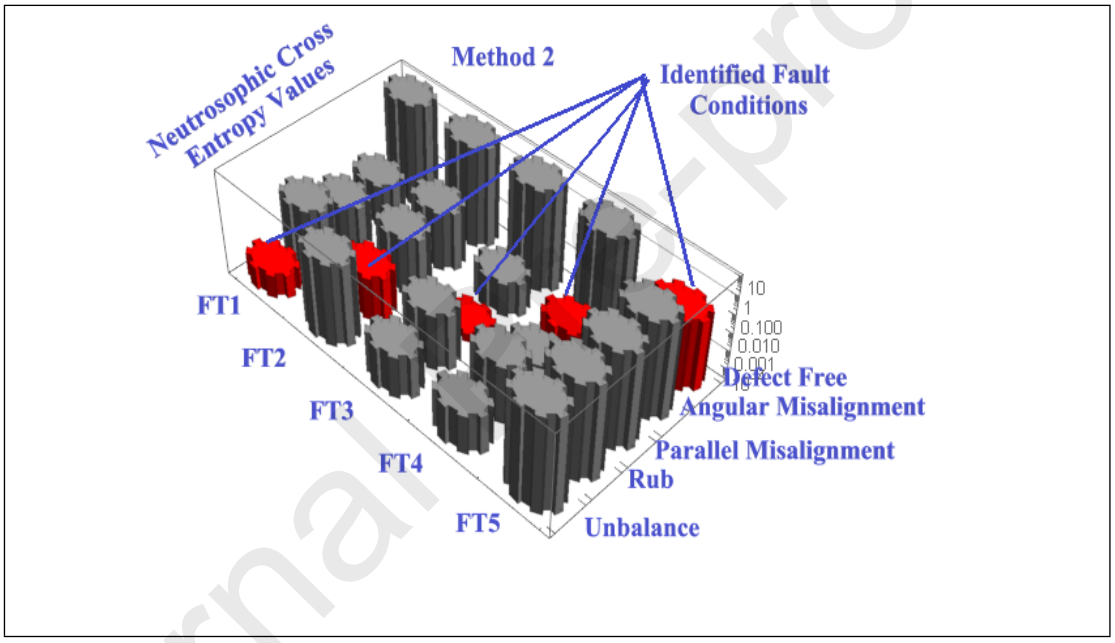

Fig. 8(c) Graphical identification of rotor defects by the proposed cross entropy measure (**Method 2**) based on single valued neutrosophic sets (SVNSs).

Fifth Diagnosis Result: - For the fifth real testing sample F_{T_5}, the various minimum symmetric cross entropy values are

$$H^{\mu}_{CE}(B_K,F_{T_5}) = 0.2264, S_{CE}(B_K,F_{T_5}) = 0.4034, T_{CE}(B_K,F_{T_5}) = 0.8903, C_B(B_K,F_{T_5}) = 0.8903$$

These values clearly correspond to the condition type F_{T_5} which is unbalance defect condition. This fact can also be experienced from **Figs.8(a, b, c, d).**

Table 8(d) Identification of rotor defects by the minimum cross entropy measure

(**Method 3**) based on bipolar neutrosophic sets (BNSs)

Entropy Measure	Bipolar Neutrosophic Cross Entropy Measure Values	Fault Diagnosis Order	Fault Condition Identified	Actual Fault Condition
$T_{CE}(B_K,F_{T_1})$	0.0010 0.2002 0.0142 0.0093 13.6899	$B_1 \succ B_4 \succ B_3 \succ B_2 \succ B_5$	Defect Free	Defect Free
$T_{CE}(B_K,F_{T_2})$	0.1966 0.0142 0.0657 0.0846 12.3635	$B_2 \succ B_4 \succ B_3 \succ B_1 \succ B_5$	Angular	Angular
$T_{CE}(B_K,F_{T_3})$	0.0155 0.0772 0.0002 0.0028 12.4013	$B_3 \succ B_4 \succ B_1 \succ B_2 \succ B_5$	Parallel	Parallel
$T_{CE}(B_K,F_{T_4})$	0.0135 0.0975 0.0041 0.0029 13.0804	$B_4 \succ B_3 \succ B_1 \succ B_2 \succ B_5$	Rub	Rub
$T_{CE}(B_K,F_{T_5})$	20.8534 17.4836 18.9610 20.0545 0.4034	$B_5 \succ B_2 \succ B_3 \succ B_1 \succ B_4$	Unbalance	Unbalance

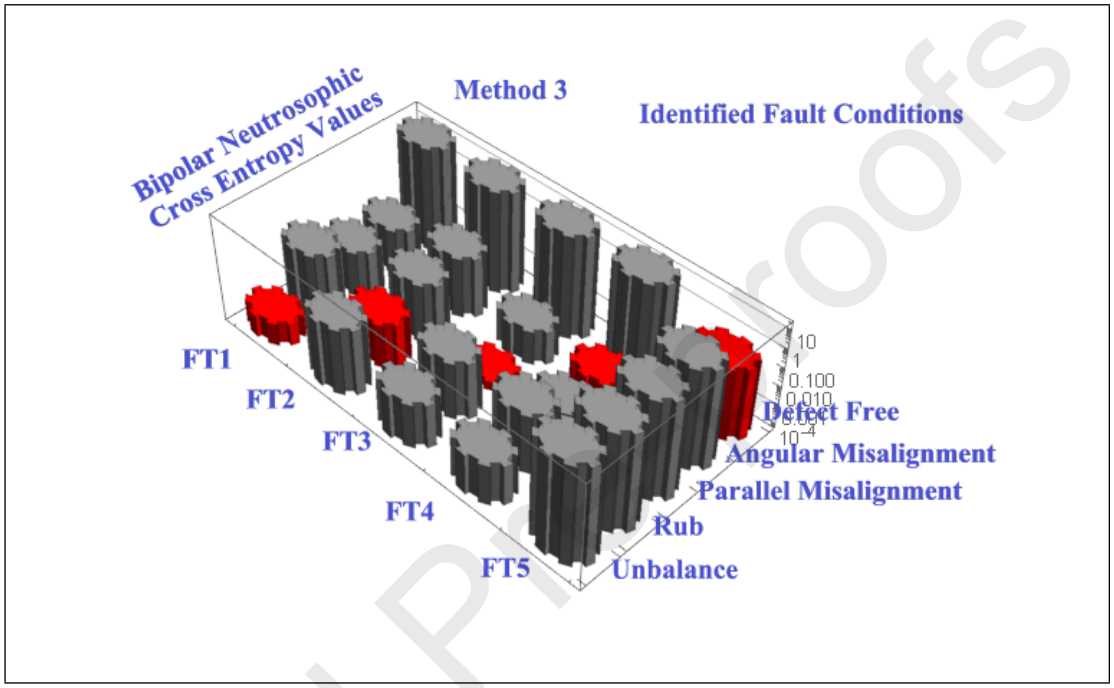

Fig. 8(d) Graphical identification of rotor defects by the proposed cross entropy measure (**Method 3**) based on bipolar neutrosophic sets (BNSs)

7.1 Comparative Analysis The proposed bipolar neutrosophic cross entropy and maximal overlap discrete wavelet packet transforms (MODWPT) based rotor defect identification methodology is found to be capable for identifying various rotor defect conditions such as defect free condition, rub, unbalance, angular misalignment of Mils 10 and parallel misalignment of Mils 10 respectively. On the other hand, the existing cosine similarity measure [1] based upon bipolar neutrosophic sets does not possess the necessary capability of identifying all rotor defects under study, especially, the rub defect condition as specified in **Table 8(a)** and **Fig. 8(a).** The justification regarding the superiority of the proposed variants of cross entropy measure, based on fuzzy sets, single valued neutrosophic sets and bipolar neutrosophic sets, over the existing cosine similarity measure based on bipolar neutrosophic sets have been well summarized in **Table 8(e).**

7.2 Intuitive Analysis To perform the intuitive analysis [36,37] of the proposed cross entropy measures of fuzzy sets, single valued neutrosophic sets and bipolar neutrosophic sets:

Table 8(e) Comparative analysis of identified rotor defect conditions employing the proposed **Methods 1- 3** and existing cosine similarity measure [42] based on bipolar neutrosophic sets (BNSs)

Table 9(a). Intuitive analysis of $H_{CE}^{\mu}(A_1,A_2)$based on fuzzy sets and existing cosine similarity measure [1] based on bipolar neutrosophic sets

Actual Fault Conditions	**Identified Fault Conditions**			
	Method 1	**Method 2**	**Method 3**	**Existing Method [42]**
Defect Free	✓	✓	✓	✓
Angular Misalignment of 10 Mils	✓	✓	✓	✓
Parallel Misalignment of 10 Mils	✓	✓	✓	✓
Rub	✓	✓	✓	Could not identify
Unbalance	✓	✓	✓	✓

Group No.	Fuzzy set A_1	Fuzzy set A_2	Value of $C_M(A_1,A_2)$	Value of $H_{CE}^{\mu}(A_1,A_2)$
1	0.0000	1.0000	0.2218	1.1507
2	0.1000	1.0000	0.0941	0.6832
3	0.2000	1.0000	0.0581	0.5239
4	0.3000	1.0000	0.0369	0.4028
5	0.4000	1.0000	0.0240	0.3020
6	0.5000	1.0000	0.0175	0.2161
7	0.6000	1.0000	0.0185	0.1436
8	0.7000	1.0000	0.0328	0.0843
9	0.8000	1.0000	0.1360	0.0393
10	0.9000	1.0000	0.1349	0.0103
11	1.0000	1.0000	0.0748	0.0000

(a) We have assumed two fuzzy sets A_1 and A_2 as shown in **Table 9(a)**. In this experiment, the value of A_2 is fixed which is $1 \cdot 0000$, meanwhile the value of A_1 has been increased gradually as shown in **Table 9(a)**. The symmetric fuzzy cross entropy values $H_{CE}^{\mu}(A_1,A_2)$ are computed employing equation (**21**) and are represented in **Table 9(a)**.

(b) We have assumed two single valued neutrosophic sets S_1 and S_2 as shown in **Table 9(b)**. In this experiment, the value of S_2 is fixed which is (1.0000,0.0100,0.0100), meanwhile the value of S_1 has been increased gradually as shown in **Table 9(b)**. The symmetric single

valued neutrosophic cross entropy measure $S_{CE}(S_1,S_2)$ values are computed employing equation (**22**) and are represented in **Table 9(b)**.

(c) We have assumed two bipolar neutrosophic sets C_1 and C_2 as shown in **Table 9(c)**. In this experiment, the value of C_2 is fixed as $(1.0000,0.0100,0.0100,-0.0200,-0.0200,-0.0200)$, meanwhile the value of C_1 has been increased gradually as shown in **Table 9(c)**. The symmetric bipolar neutrosophic cross entropy measure $T_{CE}(C_1,C_2)$ values are computed employing equation (**23**) and are represented in **Table 9(c)**.

Table 9(b). Intuitive analysis of $S_{CE}(A_1,A_2)$ based on single valued neutrosophic sets and existing cosine similarity measure [1] based on bipolar neutrosophic sets

Group No.	Single valued Neutrosophic Set S_1	Single valued Neutrosophic Set S_2	Value of $C_M(S_1,S_2)$	Value of $S_{CE}(S_1,S_2)$
1	$(0.0000,0.0200,0.0300)$	$(1.0000,0.0100,0.0100)$	0.2218	1.1510
2	$(0.1000,0.0200,0.0300)$	$(1.0000,0.0100,0.0100)$	0.0941	0.6835
3	$(0.2000,0.0200,0.0300)$	$(1.0000,0.0100,0.0100)$	0.0581	0.5242
4	$(0.3000,0.0200,0.0300)$	$(1.0000,0.0100,0.0100)$	0.0369	0.4031
5	$(0.4000,0.0200,0.0300)$	$(1.0000,0.0100,0.0100)$	0.0240	0.3023
6	$(0.5000,0.0200,0.0300)$	$(1.0000,0.0100,0.0100)$	0.0175	0.2164
7	$(0.6000,0.0200,0.0300)$	$(1.0000,0.0100,0.0100)$	0.0185	0.1439
8	$(0.7000,0.0200,0.0300)$	$(1.0000,0.0100,0.0100)$	0.0328	0.0846
9	$(0.8000,0.0200,0.0300)$	$(1.0000,0.0100,0.0100)$	0.1360	0.0396
10	$(0.9000,0.0200,0.0300)$	$(1.0000,0.0100,0.0100)$	0.1349	0.0106
11	$(1.0000,0.0200,0.0300)$	$(1.0000,0.0100,0.0100)$	0.0748	0.0003

A careful analysis of the results provided in **Tables 9(a, b c)** reveal that the trend of cross entropy measures $H^{\mu}_{CE}(A_1,A_2)$,$S_{CE}(S_1,S_2)$ *and* $T_{CE}(C_1,C_2)$ values go on decreasing with a slight increase in the values of the sets A_1, S_1 *and* C_1.In other words, with the growth of values of the fuzzy set A_1,S_1 *and* C_1, the trend of values of $H^{\mu}_{CE}(A_1,A_2)$,$S_{CE}(S_1,S_2)$ *and* $T_{CE}(C_1,C_2)$ is changing from larger to smaller. Similarly, the trend of $C_M(A_1,A_2)$ [1] is also changing from larger to smaller values. This justifies that, like the existing cosine similarity measure [1] based on BNSs, the proposed variants of bipolar neutrosophic cross entropy measure fairly furnishes the consistent and feasible results under intuitive analysis.

Table 9(c). Intuitive analysis of $T_{CE}(C_1,C_2)$ and existing cosine similarity measure [1] based on bipolar neutrosophic sets BNSs

Gp No.	Bipolar Neutrosophic Set C_1	Bipolar Neutrosophic Set C_2	Value of $C_M(C_1,C_2)$	Value of $T_{CE}(C_1,C_2)$
1	$(0.0000,0.0100,0.0100,-1.0000,-0.0100,-0.0100)$	$(1.0000,0.0100,0.0100,-0.0200,-0.0200,-0.020($	0.2218	2.0638

2	$(0.1000,0.0100,0.0100,-0.9000,-0.0100,-0.0100)$	$(1.0000,0.0100,0.0100,-0.0200,-0.0200,-0.020($	0.0941	1.1693
3	$(0.2000,0.0100,0.0100,-0.8000,-0.0100,-0.0100)$	$(1.0000,0.0100,0.0100,-0.0200,-0.0200,-0.020($	0.0581	0.8820
4	$(0.3000,0.0100,0.0100,-0.7000,-0.0100,-0.0100)$	$(1.0000,0.0100,0.0100,-0.0200,-0.0200,-0.020($	0.0369	0.6694
5	$(0.4000,0.0100,0.0100,-0.60000,-0.0100,-0.0100)$	$(1.0000,0.0100,0.0100,-0.0200,-0.0200,-0.020($	0.0240	0.4955
6	$(0.5000,0.0100,0.0100,-0.50000,-0.0100,-0.0100)$	$(1.0000,0.0100,0.0100,-0.0200,-0.0200,-0.020($	0.0175	0.3497
7	$(0.6000,0.0100,0.0100,-0.40000,-0.0100,-0.0100)$	$(1.0000,0.0100,0.0100,-0.0200,-0.0200,-0.020($	0.0185	0.2283
8	$(0.7000,0.0100,0.0100,-0.3000,-0.0100,-0.0100)$	$(1.0000,0.0100,0.0100,-0.0200,-0.0200,-0.020($	0.0328	0.1309
9	$(0.8000,0.0100,0.0100,-0.2000,-0.0100,-0.0100)$	$(1.0000,0.0100,0.0100,-0.0200,-0.0200,-0.020($	0.1360	0.0587
10	$(0.9000,0.0100,0.0100,-0.1000,-0.0100,-0.0100)$	$(1.0000,0.0100,0.0100,-0.0200,-0.0200,-0.020($	0.1349	0.0142
11	$(1.0000,0.0100,0.0100,0.0000,-0.0100,-0.0100)$	$(1.0000,0.0100,0.0100,-0.0200,-0.0200,-0.020($	0.0748	0.0005

.

6. Conclusion

This study aims at establishing of a new rotor defect identification methodology through maximal overlap discrete wavelet packet transforms (MODWPT) combined with cross entropy measures of fuzzy sets, single valued neutrosophic sets and bipolar neutrosophic sets of training and testing samples of various rotor defect conditions such as angular misalignment of 10 Mils, horizontal or parallel misalignment of 10 Mils, unbalance, rub and defect free condition respectively. The minimum fuzzy cross entropy measure (**Method 1),** single valued neutrosophic cross entropy measure (**Method 2)** and bipolar neutrosophic cross entropy measure (**Method 3)** values between various familiar rotor defect conditions B_K and fourth real testing sample F_{T_4} are computed as 0.0006, 0.0018, 0.0029 respectively. All these values clearly reflect the rub defect condition which is exactly same as experienced by the experimental investigations. This justifies that our proposed variants of bipolar neutrosophic cross entropy measures possess the necessary capability of identifying rotor defects under study. On another hand, the existing cosine similarity measure [42] based upon bipolar neutrosophic sets does not possess the necessary capability of identifying all rotor defects under study as it could not identify the rub defect condition. This justifies the superiority of our proposed bipolar neutrosophic cross entropy measure and MODWPT based methodology over the existing methodology. Under intuitive analysis, the symmetric cross entropy measure values between the assumed fuzzy sets, single valued neutrosophic sets and bipolar neutrosophic sets are computed as 1.1507,0.6832,…,0.0000; 1.1510,0.6835,…,0.0003; 2.0638,1.1693,…,0.0005 respectively. Also, the existing cosine similarity measure values between the assumed bipolar neutrosophic sets are computed as

0.2218, 0.0941,…,0.0748 respectively. The trend of all these values is changing from larger to smaller. This indicates that, like the existing cosine similarity measure [42], our proposed variants of bipolar neutrosophic cross entropy measures are equally compatible for further mathematical treatments under intuitive environment. The proposed rotor defect identification methodology is applicable for automatic assessment of defect severities when the machine is operated at constant speed. Our endeavor in future will be a subject of automatic assessment of rotor defects when the machine is operated at varying speed and different load conditions.

Acknowledgment

This work was supported by the National Natural Science Foundation of China (Nos. U1909217, U1709208), the Zhejiang Natural Science Foundation of China (No. LD21E050001), the Zhejiang Special Support Program for High-level Personnel Recruitment of China (No. 2018R52034), and the Wenzhou Major Science and Technology Innovation Project of China (No. ZG2020051).

Reference

[1] Pramanik, S., Dey, P., Smarandache, F., and Ye, J., 2018, "Cross Entropy Measures of Bipolar and Interval Bipolar Neutrosophic Sets and Their Application for Multi-Attribute Decision-Making," Axioms, **7**(2), p. 21.
[2] Wei and Li, 2019, "A Review of Early Fault Diagnosis Approaches and Their Applications in Rotating Machinery," Entropy, **21**(4), p. 409.
[3] Huachun, W., Jian, Z., Chunhu, X., Jiyang, Z., and Yiming, H., 2021, "Two-Dimensional Time Series Sample Entropy Algorithm: Applications to Rotor Axis Orbit Feature Identification," Mech. Syst. Signal Process., **147**, p. 107123.
[4] Meng, Z., Zhan, X., Li, J., and Pan, Z., 2018, "An Enhancement Denoising Autoencoder for Rolling Bearing Fault Diagnosis," Measurement, **130**, pp. 448–454.
[5] Pan, Z., Meng, Z., Chen, Z., Gao, W., and Shi, Y., 2020, "A Two-Stage Method Based on Extreme Learning Machine for Predicting the Remaining Useful Life of Rolling-Element Bearings," Mech. Syst. Signal Process., **144**, p. 106899.
[6] Meng, Z., Lv, M., Liu, Z., and Fan, F., 2021, "General Synchroextracting Chirplet Transform: Application to the Rotor Rub-Impact Fault Diagnosis," Measurement, **169**, p. 108523.
[7] Kumar, A., Gandhi, C., Liu, X., Liu, Y., Zhou, Y., Kumar, R., and Xiang, J., 2020, "A Novel Health Indicator Developed Using Filter-Based Feature Selection Algorithm for the Identification of Rotor Defects," Proc. Inst. Mech. Eng. Part O J. Risk Reliab., p. 1748006X2091695.
[8] Patel, T. H., and Darpe, A. K., 2009, "Experimental Investigations on Vibration Response of Misaligned Rotors," Mech. Syst. Signal Process., **23**(7), pp. 2236–2252.
[9] Sekhar, A. S., and Prabhu, B. S., 1995, "Effects of Coupling Misalignment on

Vibrations of Rotating Machinery," J. Sound Vib., **185**(4), pp. 655–671.
[10] Xiong, X., Yang, S., and Gan, C., 2012, "A New Procedure for Extracting Fault Feature of Multi-Frequency Signal from Rotating Machinery," Mech. Syst. Signal Process., **32**, pp. 306–319.
[11] Mereles, A., and Cavalca, K. L., 2021, "Mathematical Modeling of Continuous Multi-Stepped Rotor-Bearing Systems," Appl. Math. Model., **90**, pp. 327–350.
[12] Yan, X., Zhang, C., and Liu, Y., 2021, "Multi-Branch Convolutional Neural Network with Generalized Shaft Orbit for Fault Diagnosis of Active Magnetic Bearing-Rotor System," Measurement, **171**, p. 108778.
[13] Srinivas R, S., Tiwari, R., and Babu, Ch. K., 2020, "Modelling, Analysis and Identification of the Parallel and Angular Misalignments in a Coupled Rotor-Bearing-AMB System," J. Dyn. Syst. Meas. Control.
[14] Saavedra, P. N., and Ramírez, D. E., 2004, "Vibration Analysis of Rotors for the Identification of Shaft Misalignment Part 1: Theoretical Analysis," Proc. Inst. Mech. Eng. Part C J. Mech. Eng. Sci., **218**(9), pp. 971–985.
[15] Saavedra, P. N., and Ramírez, D. E., 2004, "Vibration Analysis of Rotors for the Identification of Shaft Misalignment Part 2: Experimental Validation," Proc. Inst. Mech. Eng. Part C J. Mech. Eng. Sci., **218**(9), pp. 987–999.
[16] Bouyer, J., and Fillon, M., 2002, "An Experimental Analysis of Misalignment Effects on Hydrodynamic Plain Journal Bearing Performances," J. Tribol., **124**(2), pp. 313–319.
[17] Chandra, N. H., and Sekhar, A. S., 2016, "Fault Detection in Rotor Bearing Systems Using Time Frequency Techniques," Mech. Syst. Signal Process., **72–73**, pp. 105–133.
[18] Sinha, J. K., 2007, "Higher Order Spectra for Crack and Misalignment Identification in the Shaft of a Rotating Machine," Struct. Health Monit. Int. J., **6**(4), pp. 325–334.
[19] Gerami, A., Fittro, R., and Knospe, C., 2020, "Improving Disturbance Rejection in Nonlinear Active Magnetic Bearing Systems: Using Lur'e Formulation," J. Dyn. Syst. Meas. Control, **142**(4), p. 041007.
[20] Xu, L., Pennacchi, P., and Chatterton, S., 2020, "A New Method for the Estimation of Bearing Health State and Remaining Useful Life Based on the Moving Average Cross-Correlation of Power Spectral Density," Mech. Syst. Signal Process., **139**, p. 106617.
[21] Wang, X., Tang, G., and He, Y., 2020, "Application of RSSD-OCYCBD Strategy in Enhanced Fault Detection of Rolling Bearing," Complexity, **2020**, pp. 1–24.
[22] Abbasi, A. R., Mahmoudi, M. R., and Arefi, M. M., 2021, "Transformer Winding Faults Detection Based on Time Series Analysis," IEEE Trans. Instrum. Meas., **70**, pp. 1–10.
[23] Xiao, C., Tang, H., Ren, Y., Xiang, J., and Kumar, A., 2021, "A Fault Frequency Bands Location Method Based on Improved Fast Spectral Correlation to Extract Fault Features in Axial Piston Pump Bearings," Measurement, **171**, p. 108734.
[24] Zhao, X., Qin, Y., He, C., and Jia, L., 2020, "Intelligent Fault Identification for Rolling Element Bearings in Impulsive Noise Environments Based on Cyclic Correntropy Spectra and LSSVM," IEEE Access, **8**, pp. 40925–40938.
[25] Abbasi, A. R., and Mahmoudi, M. R., 2021, "Application of Statistical Control Charts to Discriminate Transformer Winding Defects," Electr. Power Syst. Res., **191**, p. 106890.

[26] Wodecki, J., Michalak, A., and Zimroz, R., 2021, "Local Damage Detection Based on Vibration Data Analysis in the Presence of Gaussian and Heavy-Tailed Impulsive Noise," Measurement, **169**, p. 108400.
[27] Mauricio, A., Qi, J., Smith, W. A., Sarazin, M., Randall, R. B., Janssens, K., and Gryllias, K., 2020, "Bearing Diagnostics under Strong Electromagnetic Interference Based on Integrated Spectral Coherence," Mech. Syst. Signal Process., **140**, p. 106673.
[28] Camarena-Martinez, D., Valtierra-Rodriguez, M., Amezquita-Sanchez, J. P., Granados-Lieberman, D., Romero-Troncoso, R. J., and Garcia-Perez, A., 2016, "Shannon Entropy and K -Means Method for Automatic Diagnosis of Broken Rotor Bars in Induction Motors Using Vibration Signals," Shock Vib., **2016**, pp. 1–10.
[29] Fu, L., He, Z. Y., Mai, R. K., and Bo, Z. Q., 2009, "Approximate Entropy and Its Application to Fault Detection and Identification in Power Swing," *2009 IEEE Power & Energy Society General Meeting*, IEEE, Calgary, Canada, pp. 1–8.
[30] Zhao, L.-Y., Wang, L., and Yan, R.-Q., 2015, "Rolling Bearing Fault Diagnosis Based on Wavelet Packet Decomposition and Multi-Scale Permutation Entropy," Entropy, **17**(12), pp. 6447–6461.
[31] Leite, G. de N. P., Araújo, A. M., Rosas, P. A. C., Stosic, T., and Stosic, B., 2019, "Entropy Measures for Early Detection of Bearing Faults," Phys. Stat. Mech. Its Appl., **514**, pp. 458–472.
[32] Zhang, X., Yan, Q., Yang, J., Zhao, J., and Shen, Y., 2019, "An Assembly Tightness Detection Method for Bolt-Jointed Rotor with Wavelet Energy Entropy," Measurement, **136**, pp. 212–224.
[33] Zheng, J., Pan, H., Liu, Q., and Ding, K., 2020, "Refined Time-Shift Multiscale Normalised Dispersion Entropy and Its Application to Fault Diagnosis of Rolling Bearing," Phys. Stat. Mech. Its Appl., **545**, p. 123641.
[34] Haidong, S., Junsheng, C., Hongkai, J., Yu, Y., and Zhantao, W., 2020, "Enhanced Deep Gated Recurrent Unit and Complex Wavelet Packet Energy Moment Entropy for Early Fault Prognosis of Bearing," Knowl.-Based Syst., **188**, p. 105022.
[35] Kumar, A., Gandhi, C. P., Zhou, Y., Kumar, R., and Xiang, J., 2020, "Improved Deep Convolution Neural Network (CNN) for the Identification of Defects in the Centrifugal Pump Using Acoustic Images," Appl. Acoust., **167**, p. 107399.
[36] Kumar, A., Gandhi, C. P., Zhou, Y., Tang, H., and Xiang, J., 2020, "Fault Diagnosis of Rolling Element Bearing Based on Symmetric Cross Entropy of Neutrosophic Sets," Measurement, **152**, p. 107318.
[37] Kumar, A., Gandhi, C. P., Zhou, Y., Kumar, R., and Xiang, J., 2020, "Variational Mode Decomposition Based Symmetric Single Valued Neutrosophic Cross Entropy Measure for the Identification of Bearing Defects in a Centrifugal Pump," Appl. Acoust., **165**, p. 107294.
[38] Kumar, A., Gandhi, C. P., Tang, H., Vashishtha, G., Kumar, R., Zhou, Y., and Xiang, J., 2021, "Adaptive Sensitive Frequency Band Selection for VMD to Identify Defective Components of an Axial Piston Pump," Chin. J. Aeronaut., p. S1000936120306051.
[39] Afia, A., Rahmoune, C., Benazzouz, D., Merainani, B., and Fedala, S., 2019, "New Gear Fault Diagnosis Method Based on MODWPT and Neural Network for Feature Extraction and Classification," J. Test. Eval., **49**(2), pp. 1064–1085.
[40] Mauricio, A., and Gryllias, K., 2021, "Cyclostationary-Based Multiband Envelope Spectra Extraction for Bearing Diagnostics: The Combined Improved Envelope

Spectrum," Mech. Syst. Signal Process., **149**, p. 107150.
[41] Wang, X., Zheng, J., Pan, H., Liu, Q., and Wang, C., 2021, "Maximum Envelope-Based Autogram and Symplectic Geometry Mode Decomposition Based Gear Fault Diagnosis Method," Measurement, **174**, p. 108575.
[42] Smarandache, F., 2000, "Neutrosophic Probability, Set, And Logic (First Version)."
[43] Yang, Y., He, Y., Cheng, J., and Yu, D., 2009, "A Gear Fault Diagnosis Using Hilbert Spectrum Based on MODWPT and a Comparison with EMD Approach," Measurement, **42**(4), pp. 542–551.
[44] Shan, P.-W., and Li, M., 2010, "Nonlinear Time-Varying Spectral Analysis: HHT and MODWPT," Math. Probl. Eng., **2010**, p. e618231 [Online]. Available: https://www.hindawi.com/journals/mpe/2010/618231/. [Accessed: 11-Apr-2020].

Appendix-A.1

We set

$R_0^+ = \tilde{\mu}_{A^f}^+(x_i) + \tilde{\mu}_{B^f}^+(x_i)$, $R_1^+ = \sqrt{\tilde{\mu}_{A^f}^+(x_i)} + \sqrt{\tilde{\mu}_{B^f}^+(x_i)}$, $R_2^+ = \sqrt{1 - \tilde{\mu}_{A^f}^+(x_i)} + \sqrt{1 - \tilde{\mu}_{B^f}^+(x_i)}$;

$R_0^- = \tilde{\mu}_{A^f}^-(x_i) + \tilde{\mu}_{B^f}^-(x_i)$, $R_1^- = \sqrt{-\tilde{\mu}_{A^f}^-(x_i)} + \sqrt{-\tilde{\mu}_{B^f}^-(x_i)}$, $R_2^- = \sqrt{1 + \tilde{\mu}_{A^f}^-(x_i)} + \sqrt{1 + \tilde{\mu}_{B^f}^-(x_i)}$;

$S_0^+ = \tilde{i}_{A^f}^+(x_i) + \tilde{i}_{B^f}^+(x_i)$, $S_1^+ = \sqrt{\tilde{i}_{A^f}^+(x_i)} + \sqrt{\tilde{i}_{B^f}^+(x_i)}$, $S_2^+ = \sqrt{1 - \tilde{i}_{A^f}^+(x_i)} + \sqrt{1 - \tilde{i}_{B^f}^+(x_i)}$;

$S_0^- = \tilde{i}_{A^f}^-(x_i) + \tilde{i}_{B^f}^-(x_i)$, $S_1^- = \sqrt{-\tilde{i}_{A^f}^-(x_i)} + \sqrt{-\tilde{i}_{B^f}^-(x_i)}$, $S_2^- = \sqrt{1 + \tilde{i}_{A^f}^-(x_i)} + \sqrt{1 + \tilde{i}_{B^f}^-(x_i)}$;

$T_0^+ = \tilde{f}_{A^f}^+(x_i) + \tilde{f}_{B^f}^+(x_i)$, $T_1^+ = \sqrt{\tilde{f}_{A^f}^+(x_i)} + \sqrt{\tilde{f}_{B^f}^+(x_i)}$, $T_2^+ = \sqrt{1 - \tilde{f}_{A^f}^+(x_i)} + \sqrt{1 - \tilde{f}_{B^f}^+(x_i)}$,

$T_0^- = \tilde{f}_{A^f}^-(x_i) + \tilde{f}_{B^f}^-(x_i)$, $T_1^- = \sqrt{-\tilde{f}_{A^f}^-(x_i)} + \sqrt{-\tilde{f}_{B^f}^-(x_i)}$, $T_2^- = \sqrt{1 + \tilde{f}_{A^f}^-(x_i)} + \sqrt{1 + \tilde{f}_{B^f}^-(x_i)}$.

Appendix-A.2

We set

$U_0^+ = \mu_{B_K}^+(x_i) + \mu_{F_{T_J}}^+(x_i)$, $U_0^- = \mu_{B_K}^-(x_i) + \mu_{F_{T_J}}^-(x_i)$, $U_1^- = \sqrt{-\mu_{B_K}^-(x_i)} + \sqrt{-\mu_{F_{T_J}}^-(x_i)}$,

$U_2^- = \sqrt{1 + \mu_{B_K}^-(x_i)} + \sqrt{1 + \mu_{F_{T_J}}^-(x_i)}$,

$I_0^+ = i_{B_K}^+(x_i) + i_{F_{T_J}}^+(x_i)$, $I_1^+ = \sqrt{i_{B_K}^+(x_i)} + \sqrt{i_{F_{T_J}}^+(x_i)}$, $I_2^+ = \sqrt{1 - i_{B_K}^+(x_i)} + \sqrt{1 - i_{F_{T_J}}^+(x_i)}$,

$I_0^- = i_{B_K}^-(x_i) + i_{F_{T_J}}^-(x_i)$, $I_1^- = \sqrt{-i_{B_K}^-(x_i)} + \sqrt{-i_{F_{T_J}}^-(x_i)}$, $I_2^- = \sqrt{1 + i_{B_K}^-(x_i)} + \sqrt{1 + i_{F_{T_J}}^-(x_i)}$,

$F_0^+ = f_{B_K}^+(x_i) + f_{F_{T_J}}^+(x_i)$, $F_1^+ = \sqrt{f_{B_K}^+(x_i)} + \sqrt{f_{F_{T_J}}^+(x_i)}$, $F_2^+ = \sqrt{1 - f_{B_K}^+(x_i)} + \sqrt{1 - f_{F_{T_J}}^+(x_i)}$,

$F_0^- = f_{B_K}^-(x_i) + f_{F_{T_J}}^-(x_i)$, $F_1^- = \sqrt{-f_{B_K}^-(x_i)} + \sqrt{-f_{F_{T_J}}^-(x_i)}$, $F_2^- = \sqrt{1 + f_{B_K}^-(x_i)} + \sqrt{1 + f_{F_{T_J}}^-(x_i)}$.

Highlights

- MODWPT is employed for decomposing vibration signals.
- Some novel variants of bipolar neutrosophic cross entropy measures are proposed for identifying rotor defects.
- The proposed variants of cross entropy measure are superior and can perform well under intuitive analysis.

Credit authorship contribution statement:
Chander Parkash (C. P. Gandhi): Mathematical Investigations, Writing original draft. Anil Kumar: Writing original draft, experimental Investigations. Govind Vashishtha: Visualization. Ravi Kant: Visualization. Jiawei Xiang: Writing, review & editing, Supervision.

Declaration of Interest

The authors declare that they have no known competing financial interests or personal relationships that could have appeared to influence the work reported in this paper.